

Alkoxyurea-Based Histone Deacetylase Inhibitors Increase Cisplatin Potency in Chemoresistant Cancer Cell Lines

Katharina Stenzel,^{†,○} Alexandra Hamacher,^{†,○} Finn K. Hansen,^{†,‡,Ⓛ} Christoph G. W. Gertzen,[†] Johanna Senger,[§] Viktoria Marquardt,^{†,||,Ⓛ,#} Linda Marek,^{†,||} Martin Marek,[∇] Christophe Romier,[∇] Marc Remke,^{||,Ⓛ,#} Manfred Jung,^{§,Ⓛ} Holger Gohlke,^{†,Ⓛ} Matthias U. Kassack,^{*,†,◆} and Thomas Kurz^{*,†,◆,Ⓛ}

[†]Institut für Pharmazeutische und Medizinische Chemie, Heinrich-Heine-Universität Düsseldorf, Universitätsstraße 1, 40225 Düsseldorf, Germany

[‡]Pharmaceutical/Medicinal Chemistry, Institute of Pharmacy, Leipzig University, Brüderstraße 34, 04103 Leipzig, Germany

[§]Institut für Pharmazeutische Wissenschaften, Albert-Ludwigs-Universität Freiburg, Albertstraße 25, 79104 Freiburg, Germany

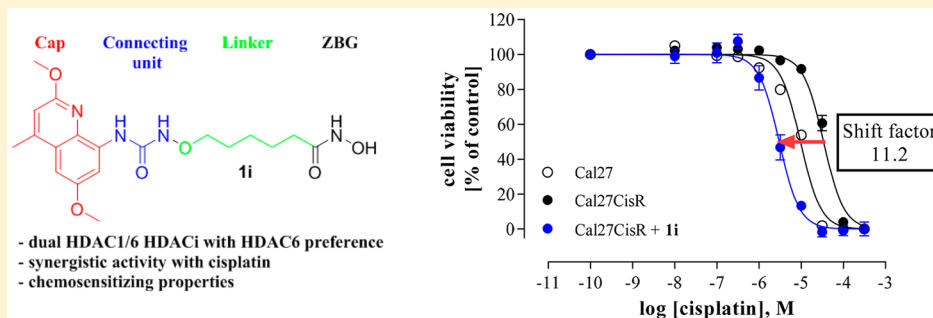
^{||}Department of Pediatric Oncology, Hematology, and Clinical Immunology, Medical Faculty, Heinrich-Heine-University, Moorenstraße 5, 40225 Düsseldorf, Germany

[Ⓛ]Department of Neuropathology, Medical Faculty, Heinrich-Heine-University, Moorenstraße 5, 40225 Düsseldorf, Germany

[#]Division of Pediatric Neuro-Oncogenomics, German Cancer Consortium (DKTK) and German Cancer Research Center (DKFZ), Moorenstraße 5, 40225 Düsseldorf, Germany

[∇]Département de Biologie Structurale Intégrative, Institut de Génétique et Biologie Moléculaire et Cellulaire (IGBMC), Université de Strasbourg (UDS), CNRS, INSERM, 1 Rue Laurent Fries, 67404 Illkirch Cedex, France

Supporting Information



ABSTRACT: The synthesis and biological evaluation of potent hydroxamate-based dual HDAC1/6 inhibitors with modest HDAC6 preference and a novel alkoxyurea connecting unit linker region are described. The biological studies included the evaluation of antiproliferative effects and HDAC inhibitory activity in the human ovarian cancer cell line A2780, the human squamous carcinoma cell line Cal27, and their cisplatin resistant sublines A2780CisR and Cal27CisR. The three most potent compounds **1g–i** showed IC_{50} values in the low μ M and sub- μ M range. **1g–i** revealed low nM IC_{50} values for HDAC6 with up to 15-fold preference over HDAC1, >3500-fold selectivity over HDAC4, and >100-fold selectivity over HDAC8. Furthermore, their ability to enhance cisplatin sensitivity was analyzed in Cal27 and Cal27CisR cells. Notably, a 48 h preincubation of **1g–i** significantly enhanced the antiproliferative effects of cisplatin in Cal27 and Cal27CisR. **1g–i** interacted synergistically with cisplatin. These effects were more pronounced for the cisplatin resistant subline Cal27CisR.

INTRODUCTION

The dynamic histone acetylation/deacetylation state is regulated by histone acetyltransferases (HATs) and histone deacetylases (HDACs). HDACs are clinically validated cancer targets and represent a group of 18 enzymes catalyzing the removal of acetyl groups from *N*-acetyl-lysine residues of histones and various non-histone proteins during post-translational protein modification.¹ Deacetylation causes chromatin condensation leading mainly to transcriptional suppression, whereas acetylation leads to gene activation. HDACs of classes I (HDACs 1–3, 8), IIa (HDACs 4, 5, 7, 9), IIb (HDACs 6, 10), and IV (HDAC 11) are

Zn²⁺ dependent enzymes. Class III HDACs (sirtuins) are NAD⁺ dependent deacetylases.²

HDAC inhibition can abrogate aberrant epigenetic changes associated with cancer.³ Currently, four histone deacetylase inhibitors (HDACi), vorinostat (cutaneous T-cell lymphoma; CTCL), romidepsin (CTCL and peripheral T-cell lymphoma; PTCL), belinostat (relapsed or refractory PTCL), and panobinostat (multiple myeloma; MM) have been approved

Received: December 8, 2016

Published: June 5, 2017

for cancer treatment by the FDA (Figure 1).⁴ Moreover, the class I selective benzamide-based HDACi chidamide has recently been

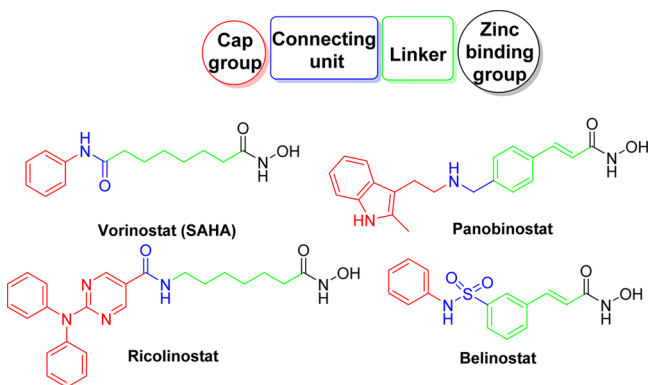


Figure 1. General pharmacophore model of HDACi.

approved in China for the treatment of relapsed or refractory PTCL.⁵ Furthermore, HDACi are under investigation for potential application as therapeutic drugs for treating a variety of diseases beyond cancer including inflammation, HIV, neurodegenerative diseases, and parasitic diseases such as malaria and schistosomiasis.^{1,6} Structurally, most HDACi are characterized by a widely accepted pharmacophore model (see Figure 1) and contain (i) a cap group (CAP) that interacts with residues at the entry point of the active site tunnel, (ii) a linker region plus a connecting unit (CU), interacting mainly with hydrophobic residues of the tunnel, and (iii) a zinc binding group (ZBG) that coordinates the catalytically essential Zn^{2+} ion at the active site. Recent results have shown that all units have an impact on the isoform profile of HDACi.⁷

Most of the first generation HDACi are pan inhibitors. To date, it is still under debate whether pan HDAC inhibitors or class-selective HDAC inhibitors will be more effective in clinical trials regarding both safety and efficacy.⁸ To address the question if pan- or class/subtype selective HDAC inhibitors show superior clinical benefit, the development of isoform and class-selective HDACi has attracted the attention of academia and industry.⁹ Experimental preclinical and clinical data suggest that the combination of HDACi with established DNA-modifying anticancer drugs (e.g., cisplatin, carboplatin, temozolomide) provides synergistic effects in the treatment of hematological and solid tumors, possibly through HDACi-mediated increased accessibility of DNA or inhibition of antiapoptotic gene expression.¹⁰

Recently, ricolinostat (ACY-1215, Figure 1), an HDAC6 preferential inhibitor with additionally potent inhibitory activity toward class I HDACs, has entered phase II clinical trials for the treatment of multiple myeloma and lymphoid malignancies.¹¹ HDAC6 is structurally unique and acts primarily via deacetylation of non-histone proteins such as α -tubulin and Hsp90. HDAC6 contains two catalytic domains and a C-terminal zinc finger region responsible for binding of ubiquitinated proteins. In addition, HDAC6 possesses a significantly wider channel rim compared to other HDACs. Therefore, HDAC6 selective inhibitors often contain bulky or branched cap groups. Moreover, an sp^2 -hybridized carbon atom in α -position related to the ZBG is often present in HDAC6-preferential and -selective HDACi.¹² The hydroxamic acid group and the α -mercaptoacetamide moiety are typical ZBGs of HDAC6-selective HDACi.¹³

Dual inhibitors, inhibiting HDAC6 and to a lesser extent HDAC class I, would help to decrease unwanted (cytotoxic) side effects of class I and still make use of beneficial effects associated with HDAC6 inhibition. We now discovered that alkoxyurea-based HDACi with quinoline cap groups can serve as potent dual HDAC1/6 inhibitors, with moderate HDAC6 preference. Herein, we report the structure-based design, straightforward synthesis, and biological evaluation of this class of HDACi with potent anticancer activity and remarkable chemosensitizing properties. Compounds were evaluated in the human ovarian cancer cell line A2780 and the adenocarcinoma cell line Cal27 and their cisplatin resistant sublines A2780CisR and Cal27CisR for antiproliferative effects and inhibition of cellular HDAC activity. Compounds **1g–i** were further tested for inhibition of selected HDAC isoforms (1, 4, 6, and 8, respectively). Molecular modeling and docking studies were performed to rationalize the observed selectivity profile. The acetylation of α -tubulin and histone H3 was analyzed in Cal27 and Cal27CisR to show HDAC6 inhibition in a complex cellular environment. Eventually, **1g–i** were shown to enhance cisplatin sensitivity in Cal27 and Cal27CisR in a synergistic manner.

RESULTS AND DISCUSSION

Design of HDAC6-Preferential HDACi with an Alkoxyurea Connecting Unit Linker Region. Recently, we studied the effects of a small library of HDACi containing alkoxyamide and alkoxyurea connecting-unit linker regions in cellular MTT and pan-HDAC assays on sensitive and chemoresistant cancer cell lines.¹⁴ Initial studies on alkoxyurea **1a** revealed only moderate cytotoxicity assessed in MTT assay against the human ovarian cancer cell lines A2780 ($IC_{50} = 10.8 \mu M$) and A2780CisR ($IC_{50} = 11.6 \mu M$) but significant HDAC inhibition in a cellular HDAC assay targeting class I and class IIb HDACs in A2780 ($IC_{50} = 1.07 \mu M$) and A2780CisR ($IC_{50} = 0.85 \mu M$).¹⁴ Due to the presence of a bulky cap group and structural similarities with ricolinostat (Figure 1), we hypothesized that **1a** might show a comparable isoform profile with preferred HDAC6 inhibition. Subsequent isoform profiling confirmed our hypothesis and revealed potent activity against HDAC6 and preference over HDACs 1, and 8 (Table 1). **1a** did not show any inhibition of HDAC4. The pan inhibitor vorinostat and the class IIa selective trifluoromethylloxadiazole (TFMO)-HDACi TMP269 were used as reference HDACi.¹⁵ On the basis of these preliminary results,

Table 1. Inhibition Activities of Compound **1a** and Vorinostat against HDAC Isoforms 1, 4, 6, and 8^a

Compound	Structure	IC_{50} [nM] of HDAC isoforms			
		HDAC1	HDAC4	HDAC 6	HDAC8
1a		189 ± 20.4	>10000	51.7 ± 4.1	11170 ± 2220
vorinostat		45 ± 8	n.d.	108 ± 11	1260 ± 210
TMP269		n.d.	447 ± 30	n.d.	n.d.

^aValues of HDAC1, -6, and -8 are the mean ± SD of three independent experiments. Values for HDAC4 were determined in duplicate by Reaction Biology Corp. (Malvern, PA, USA). n.d. = not determined.

we performed a docking study in order to understand the selectivity profile of compound **1a** and to design improved analogues.

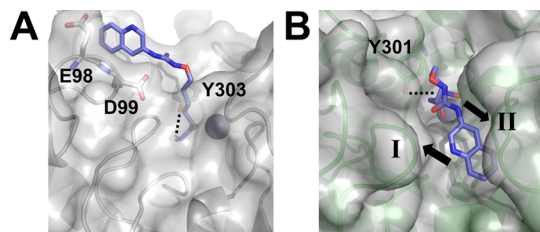


Figure 2. Docking poses for **1a** identified in HDAC1 (A) and HDAC6 (B). Hydrogen bonds are shown with dashed lines; the zinc ion is shown as a sphere. Black arrows and roman numerals indicate hydrophobic subpockets in the crevice of HDAC6.

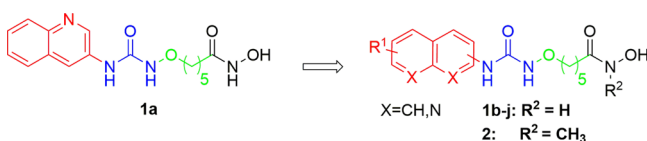


Figure 3. Lead compound **1a** and target compounds.

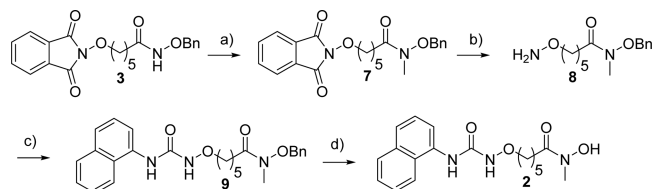
Docking of 1a and Design of 1a Derivatives. In order to understand the selectivity profile of compound **1a**, the compound was docked into the crystal structures of HDAC1 and -4, and homology models of the second catalytic domain of HDAC6 with Y301 flipped in and out. Templates for the homology modeling of HDAC6 encompass structures resulting in Y301 (numbering based on the homology model) flipped in and out. The homology models of HDAC6 had been generated and then subjected to 1 μ s of molecular dynamics simulations for identification of conformationally preferred states previously.¹⁶ X-ray crystal structures of human and zebrafish HDAC6 (PDB codes 5EDU¹⁷ and 5EF8¹⁷) have been released prior to submission of this manuscript.^{17,18} Our homology model is very similar to the crystal structures, as shown by a C α atom rmsd of 1.39 Å (1.56 Å) and a binding pocket (residues within 5 Å of the cocrystallized ligand) heavy atom rmsd of 1.75 Å (1.62 Å) toward the human (zebrafish) HDAC6 structure. This demonstrates the quality of our comparative modeling,¹⁶ although docking into HDAC6 crystal structures may further improve the accuracy of predicting binding modes of HDACi in HDAC6 in the future. HDACi were docked into both possible conformers of HDAC6. For docking, AutoDock3 in combination with DrugScore¹⁹ was used, as successfully applied previously.²⁰ No valid binding mode in which the zinc ion was complexed by the hydroxamic acid moiety was identified when docking **1a** to

HDAC4, in line with the experimental results (Table 1). Furthermore, the docking energies of **1a** in HDAC1 (−11.61 kcal mol^{−1}) are higher than those in HDAC6 (−13.48 kcal mol^{−1}) with Y301 flipped in (Table 5), which agrees qualitatively with the trend in IC₅₀ values (Table 1). In both HDAC isoforms, the zinc ion is complexed by the hydroxamic acid moiety of **1a**, and this moiety forms a hydrogen bond with Y303 and Y301 in HDAC1 and HDAC6, respectively. In contrast, the aromatic rings bind to different locations in both isoforms (Figure 2). In HDAC1, the quinoline ring binds to a small recess on the surface, which is partially lined by acidic residues on one side (Figure 2A). As to (de)solvation effects, this is energetically less favorable than if the recess was lined with hydrophobic residues. In HDAC6, the quinoline ring binds to a deeper crevice at the side of HDAC6 (Figure 2B), which is lined with hydrophobic residues. Together, this can explain the differences in the docking energies and IC₅₀ values of **1a** toward HDAC1 and -6. Notably, the crevice displays small hydrophobic subpockets I and II adjacent to the quinoline moiety (Figure 2B, black arrows). We thus hypothesized that derivatives of **1a** with a quinolyl moiety substituted with small hydrophobic groups will fill these subpockets, which will yield higher affinities toward HDAC6.

On the basis of the results of the docking study, we designed and synthesized a series of **1a** analogues as potential HDAC6i (Figure 3) and focused our structural modifications on the cap. Notably, we aimed at the replacement of the unsubstituted 3-quinolyl cap by (substituted) 4-quinolyl, 8-quinolyl, 1-naphthyl, and 2-naphthyl caps. In order to address the above-mentioned subpockets in the crevice of HDAC6, we intended to decorate selected compounds in positions 2, 4, and 6 of the quinoline moiety.

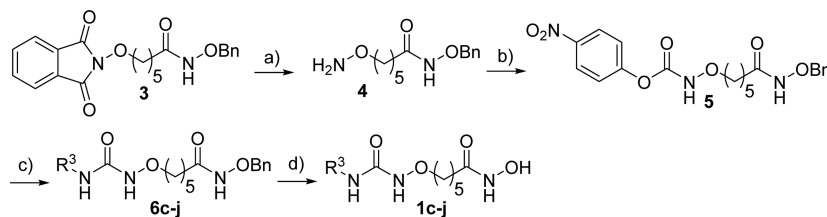
Chemistry. The synthesis of the alkoxyurea-based HDACi **1a** and **1b** has been reported previously. The synthetic protocols for the preparation of all novel HDACi are summarized in Schemes 1 and 2. The HDACi **1c–j** were prepared according to a novel and

Scheme 2. Synthesis of the Target Compound **2**^a



^aReagents and conditions: (a) CH₃I, NaH (60%), THF, rt, 16 h; (b) methylhydrazine, CH₂Cl₂, −10 °C, 3 h; (c) 1-naphthyl isocyanate, CH₂Cl₂, rt; (d) Pd/C, H₂ (1 bar), MeOH, rt, 3 h.

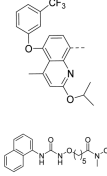
Scheme 1. Synthesis of the Target Compounds **1c–j**^a



^aReagents and conditions: (a) methylhydrazine, CH₂Cl₂, −10 °C, 3 h; (b) pyridine, CH₂Cl₂, ClCO₂C₆H₄NO₂, rt, 3 h; (c) R³NH₂, Et₃N, THF, microwave, 70 °C, 0.5 h; (d) Pd/C, H₂ (1 bar), MeOH, rt, 3 h.

straightforward synthetic protocol. The key intermediate **4** was obtained by deprotection of the readily available starting material

Table 2. Antiproliferative Effects of 1a–j, 2, Cisplatin, Tubastatin A, and Vorinostat in A2780, Cal27, and Their Cisplatin Resistant Sublines A2780CisR and Cal27CisR^b

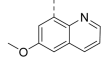
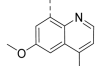
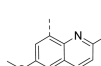
Compound	R ³	Cytotoxicity IC ₅₀ [μM]			
		A2780	A2780CisR	Cal27	Cal27CisR
1a		10.8 ± 1.0	11.6 ± 0.8	3.0 ± 0.3	5.4 ± 0.5
1b		7.6 ± 0.6	7.9 ± 0.6	1.6 ± 0.1	3.9 ± 0.4
1c		1.4 ± 0.1	1.6 ± 0.1	1.7 ± 0.1	2.3 ± 0.2
1d		27.3 ± 1.0	10.5 ± 0.8	5.8 ± 0.5	7.6 ± 0.6
1e		3.0 ± 0.3	1.0 ± 0.09	1.1 ± 0.1	2.2 ± 0.2
1f		4.3 ± 0.3	1.3 ± 0.1	2.2 ± 0.2	4.7 ± 0.3
1g		1.2 ± 0.1	0.4 ± 0.03	0.9 ± 0.04	1.3 ± 0.1
1h		1.1 ± 0.09	0.3 ± 0.02	0.6 ± 0.04	1.3 ± 0.06
1i		0.8 ± 0.07	0.4 ± 0.03	1.0 ± 0.08	1.3 ± 0.08
1j		1.7 ± 0.09	3.6 ± 0.3	3.9 ± 0.1	2.9 ± 0.2
2		46.8 ± 2.8	44.2 ± 3.7	43.7 ± 3.8	65.8 ± 5.9
cisplatin		1.88 ± 0.06	13.7 ± 1.1	2.27 ± 0.2	19.8 ± 1.1
vorinostat		2.42 ± 0.2 ^a	3.12 ± 0.3 ^a	1.98 ± 0.1	1.75 ± 0.1
tubastatin A		n.d.	n.d.	4.6 ± 0.4	10.8 ± 1.0

^aData taken from ref 14. ^bValues are the mean ± SD of three independent experiments. n.d. = not determined.

3 (see Supporting Information for details). Initial attempts to introduce the alkoxyurea moiety using 1,1'-carbonyldiimidazole (CDI) mediated or 1,1'-carbonylditriazole (CDT) mediated coupling protocols²¹ did not provide the targeted asymmetrical alkoxyureas **6** at all, or only in a low yield, especially in the case of the aminoquinoline-based cap groups. Thus, we decided to develop an optimized protocol. The aminoxy group of compound **4** was activated using 4-nitrophenyl chloroformate to obtain the 4-nitrophenyl carbamate **5**.

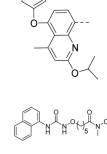
The treatment of **5** with aminoquinolines or 2-naphthylamine under conventional reaction condition provided the desired alkoxyureas only in moderate yields (33–69%) and required relatively long reaction times. We therefore considered microwave heating in order to improve reaction times and yields. Best results were obtained at 70 °C and 100 W for 0.5 h. This microwave-assisted protocol allowed the synthesis of the alkoxyureas **6c–j** in good to excellent yield (83–91%). The

Table 3. Antiproliferative Effects of 1g–i, Cisplatin, and Vorinostat in Med8a and ONS76^a

Compound	R ³	Cytotoxicity IC ₅₀ [μM]	
		Med8a	ONS76
1g		1.21 ± 0.09	2.67 ± 0.21
1h		0.60 ± 0.11	0.59 ± 0.04
1i		0.59 ± 0.06	0.65 ± 0.03
cisplatin		2.81 ± 0.51	10.2 ± 0.62
vorinostat		1.34 ± 0.18	2.04 ± 0.08

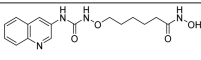
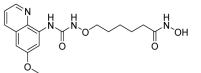
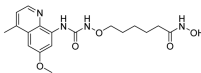
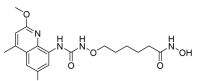
^aValues are the mean ± SD of three to four independent experiments.

Table 4. HDAC Inhibition of 1a–j, 2, Cisplatin, and Vorinostat in A2780, A2780CisR, Cal27, and Cal27CisR^a

Compound	R ³	HDAC inhibition IC ₅₀ [μM]			
		A2780	A2780 CisR	Cal27	Cal27 CisR
1a		1.1 ± 0.1	0.9 ± 0.06	1.3 ± 0.08	1.3 ± 0.07
1b		1.1 ± 0.03	0.9 ± 0.05	1.1 ± 0.04	1.0 ± 0.06
1c		5.1 ± 0.4	1.6 ± 0.1	1.0 ± 0.08	1.0 ± 0.09
1d		2.4 ± 0.2	2.0 ± 0.2	1.4 ± 0.1	1.1 ± 0.1
1e		2.1 ± 0.1	0.9 ± 0.06	0.9 ± 0.04	0.9 ± 0.06
1f		3.3 ± 0.2	1.7 ± 0.1	3.4 ± 0.3	2.8 ± 0.2
1g		1.0 ± 0.06	0.5 ± 0.02	0.9 ± 0.06	0.7 ± 0.07
1h		0.9 ± 0.05	0.4 ± 0.02	0.6 ± 0.05	0.5 ± 0.05
1i		1.7 ± 0.07	0.5 ± 0.03	0.5 ± 0.04	0.5 ± 0.04
1j		149 ± 11	n.e	107 ± 10	56 ± 1.2
2		--	--	190 ± 16	204 ± 20
vorinostat		1.68 ± 0.04	2.82 ± 0.2	0.88 ± 0.05	0.75 ± 0.06
tubastatin A		n.d.	n.d.	16.1 ± 0.9	12.1 ± 0.4

^aValues are the mean ± SD of three independent experiments. n.d. = not determined.

Table 5. Inhibitory Activities of 1a, 1g, 1h, and 1i against Human HDAC1, HDAC4, HDAC6, and HDAC8^a

Compound	Structure	IC ₅₀ [nM] of HDAC isoforms			
		HDAC1	HDAC4	HDAC6	HDAC8
1a		189 ± 20.4	>10000	51.7 ± 4.1	11170 ± 2220
1g		51.9 ± 6.2	>10000	6.10 ± 1.5	1080 ± 120
1h		77.3 ± 6.2	>10000	24.8 ± 5.2	1220 ± 290
1i		43.2 ± 3.2	>10000	2.80 ± 0.6	1540 ± 140
vorinostat		45 ± 8	n.d.	108 ± 11	1260 ± 210
TMP269		n.d.	447 ± 30	n.d.	n.d.

^aValues of HDAC1, -6, and -8 are the mean ± SD of three independent experiments. Values for HDAC4 were determined in duplicate by Reaction Biology Corp. (Malvern, PA, USA). n.d. = not determined.

subsequent catalytic hydrogenation followed by purification by flash column chromatography afforded the novel alkoxyurea-based HDACi 1c–j in 54–72% yield (Scheme 1).

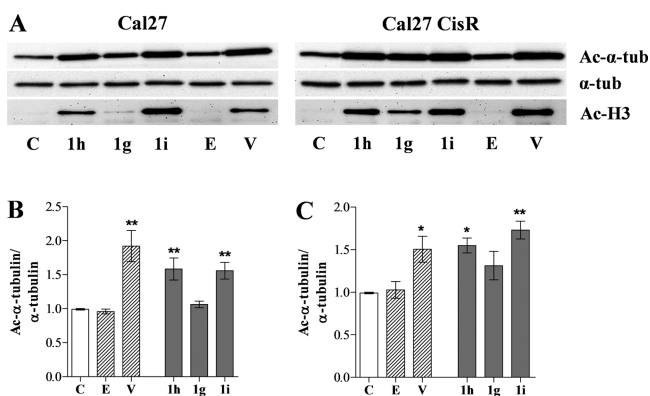


Figure 4. Compound-induced α -tubulin and histone H3 acetylation in Cal27 and Cal27CisR. (A) Representative immunoblot analysis of α -tubulin (α -tub), acetylated α -tubulin (Ac- α -tub), and acetylated histone H3 (Ac-H3) in Cal27 and Cal27CisR after compound incubation. Cal27 and Cal27CisR cells were incubated for 24 h with vehicle (C) or 1 μ M entinostat (E), vorinostat (V), 1h, 1g, or 1i, respectively. (B, C) Quantification of the immunoblots confirmed a significant increase in acetylated α -tubulin for 1h and 1i. Densitometric analysis of the protein bands of Cal27 (B) and Cal27CisR (C) were performed using ImageJ software (NIH). Data are the mean ± SD, $n = 3$. All values have been normalized to control. Statistical analysis was performed using one-way ANOVA test (***) $p < 0.05$ and (***) $p < 0.01$.

The *N*-methyl-substituted hydroxamic acid 2 was synthesized from the starting material 3 (Scheme 2). First, 3 was methylated with methyl iodide in the presence of sodium hydride as a base to obtain the *O*-protected *N*-methylated hydroxamic acid 7. The deprotection of the phthaloyl group afforded the aminoxy derivate 8, which was converted into the alkoxyurea derivate 9. Finally, the target compound 2 was obtained by catalytic hydrogenation (54% yield, Scheme 2).

Biological Evaluation. Determination of Antiproliferative Effects. Compounds 1c–j and 2 were first tested by MTT assay for antiproliferative effects in A2780 and Cal27, and their cisplatin resistant sublines A2780CisR and Cal27CisR. Results are presented in Table 2 together with vorinostat, tubastatin A, and cisplatin as controls. The compounds with the highest antiproliferative activity against all four cell lines are the 8-quinolyl-substituted analogues 1g–i showing IC₅₀ values in the range of 0.4–1.3 μ M. Notably, 1g–i are more active against A2780CisR compared to the native cell line A2780. In comparison to the lead structure 1a, the pan-HDACi vorinostat and 1g–i displayed higher antiproliferative effects whereas the HDAC6-selective HDACi tubastatin A was clearly less potent. The MTT assay revealed that the antiproliferative potential of the unsubstituted 2-naphthyl analogue 1c is almost comparable to the unsubstituted 8-quinolyl derivative 1e. In contrast, the 6-quinolyl derivative 1d and the 1-naphthyl derivative 1b are significantly less cytotoxic than 1c and 1e.

For further evaluation of the antiproliferative potential of this novel class of HDACi, the three most potent compounds (1g–i) were additionally tested for their efficacy in the two medulloblastoma cell lines Med8a and ONS76. The cell viability was determined after a 72 h incubation by Celltiter-Glo assay (Promega). The results presented in Table 3 underline the higher cytotoxicity of the compounds 1h,i compared to cisplatin and the pan-HDAC inhibitor vorinostat.

Cellular HDAC Inhibition. Cellular HDAC assays were performed as previously published.¹⁴ The results are summarized in Table 4. 1g–i displayed the most potent HDAC inhibitory activity with IC₅₀ values in the range of 0.4–1.7 μ M against all four cell lines. These results were in good agreement with the antiproliferative effects obtained with the MTT assay in the same cell lines, whereas the lead structure 1a displayed increased HDAC inhibition in comparison to its antiproliferative effects. Cellular HDAC inhibition was similar in native and resistant cell lines, whereas 1c and 1e–i showed a 2- to 3.4-fold higher activity in the cisplatin resistant subline A2780CisR compared to the native A2780.

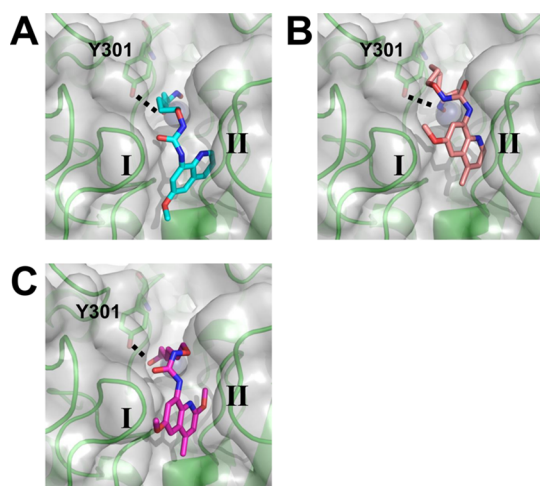


Figure 5. Docking poses for **1g** (A), **1h** (B), and **1i** (C) identified in HDAC6. Hydrogen bonds are shown as dashed lines; the zinc ion is shown as a sphere. The hydrophobic subpockets are numbered with roman numerals.

Table 6. Docking Energies for HDACi Binding to HDAC Isoforms

compd	HDAC1 ^a	HDAC4 ^a	HDAC6 ^a	HDAC8 ^a
1a	-11.61	n/a ^b	-13.48	
1g	-12.67	n/a ^b	-15.67	n/a ^b
1h	-13.36	n/a ^b	-14.52	n/a ^b
1i	-14.02	n/a ^b	-15.61	n/a ^b

^aDocking energy of the energetically most favorable configuration in the largest cluster; in kcal·mol⁻¹. ^bNo docking configuration fulfilling the criteria given in the methods section could be identified.

Inhibition of HDAC1, HDAC4, HDAC6, and HDAC8.

MTT and cellular HDAC assays identified **1g–i** as the most potent compounds. **1g–i** were therefore subjected to isoform profiling against human HDAC1, HDAC4, HDAC6, and HDAC8. Results are shown in Table 5. **1g–i** are nanomolar potency HDAC6 inhibitors (IC₅₀ in the range of 2.8–24.8 nM) and 2- to 18-fold more potent than the lead structure **1a**. **1i** demonstrated excellent selectivity over HDAC8 (SI = 550) and a preference over HDAC1 (SI = 15). HDAC6 inhibitory activity of **1i** was 2- to 9-fold higher than for **1g** and **1h** and even 18-fold higher in comparison to the lead structure **1a**.

To confirm HDAC6 inhibition in a more complex cellular environment, α -tubulin acetylation was analyzed after a 24 h incubation of 1 μ M **1g–i** in Cal27 and Cal27CisR cells. Furthermore, the ability of the potential HDAC inhibitors **1g–i** to enhance the acetylation of histone H3 was analyzed. The results of a representative Western blot analysis are shown in Figure 4.

1g–i, and vorinostat induced an accumulation of acetylated α -tubulin in comparison to the untreated control in both cell lines. This indicates that all three compounds and the reference pan-HDACi vorinostat inhibit HDAC6, whereas the HDAC1 and HDAC3 isoform-specific HDACi entinostat did not influence the amount of acetylated α -tubulin after a 24 h incubation. The α -tubulin acetylation of **1h** and **1i** was significant in comparison to the untreated control in Cal27 and Cal27CisR cells.

Furthermore, **1g–i** and vorinostat induced histone H3 acetylation indicating that they act not only as HDAC6 inhibitors. This is further supported by the fact that highly

Table 7. IC₅₀ Values (μ M) after Treatment of Cal27 and Cal27CisR with Cisplatin or in Combination with 1 μ M **1g**, 0.5 μ M **1h**, or 0.5 μ M **1i**, Respectively^a

compd	cell line			
	Cal27		Cal27CisR	
	IC ₅₀	SF	IC ₅₀	SF
cisplatin	9.13 \pm 0.5		46.4 \pm 3.1	
cisplatin + 1g 1.0 μ M	1.28 \pm 0.1	7.1	5.47 \pm 0.4	8.5
cisplatin + 1h 0.5 μ M	1.49 \pm 0.1	6.1	5.68 \pm 0.3	8.2
cisplatin + 1i 0.5 μ M	1.05 \pm 0.1	8.7	4.16 \pm 0.4	11.2
cisplatin + SAHA 1 μ M			6.80 \pm 0.2	6.8
cisplatin + tub A 10 μ M	8.30 \pm 0.2	1.1	32.0 \pm 0.3	1.5

^aSF means shift factor and was calculated as the ratio of the IC₅₀ of cisplatin alone and the IC₅₀ of the corresponding drug combination. Data shown are the mean \pm SEM of pooled data from at least three independent experiments each carried out in triplicates. All shift factors are significant (*t* test, *p* < 0.05) except for cisplatin plus tubastatin A. The used concentrations of **1g–i** were chosen on the basis of their HDAC inhibitory activity (Table 2).

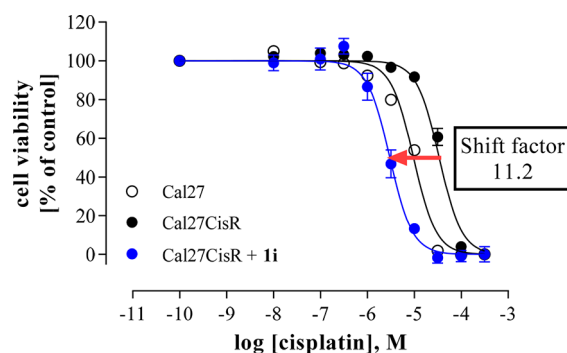


Figure 6. Treatment with **1i** restores cisplatin sensitivity of Cal27CisR cells. Cal27 (○) or Cal27CisR (●) were treated with increasing concentrations of cisplatin for 72 h. The IC₅₀ values for each cell line were determined by MTT assay. Treatment of Cal27CisR with 500 nM of **1i** 48 h prior cisplatin administration (blue dot) was able to reduce the IC₅₀ value even below the IC₅₀ of the parental cell line Cal27. The shift factor was calculated as the ratio of the IC₅₀ of cisplatin alone and the IC₅₀ of the corresponding combination with **1i** (Table 7). Data shown are the mean \pm SEM of four independent experiments each performed in triplicates.

selective HDAC6 inhibitors show only weak growth inhibition of cancer cells.²² H3 acetylation was more pronounced for **1h** and **1i**, whereas **1g** induced only a moderate acetylation of the histone core. **1g–i** showed the same or higher H3 acetylation than vorinostat. Histone acetylation induced by **1g–i** and vorinostat was more pronounced in Cal27CisR cell line than in the native cell line Cal27. Thus, acetylated H3 and acetylated tubulin levels found for **1g–i** in Figure 4 revealed that inhibition of both HDAC1 and HDAC6 may contribute to the enhancement of cisplatin chemosensitivity. Additionally, Asgar et al. reported about synergistic anticancer effects of cisplatin and vorinostat on cholangiocarcinoma cell lines.²³ Interestingly, the 24 h incubation with the class I selective HDACi entinostat resulted only in a very weak histone H3 acetylation. This unexpected effect could be attributed to the incubation time used because entinostat showed an increase of histone H3 acetylation only after a longer incubation period of 36 h.²⁴

Docking Studies. We docked compounds **1g–i** into HDACs 1, 4, 6 (with Y301 in the flipped-in conformation),

Table 8. Synergism Studies between Cisplatin and **1g–i**^a

compd [nM]	Cal27					Cal27CisR				
	cisplatin [μ M]					cisplatin [μ M]				
	0.316	0.5	1	2	5	1	3.16	5	10	20
1g										
500	0.86	0.87	0.67	0.49	0.35	*	*	0.96	0.36	0.35
600	0.79	0.77	0.57	0.37	0.34	*	*	0.60	0.36	0.37
700	*	0.97	0.63	0.43	0.32	*	0.56	0.41	0.33	0.37
800	*	0.93	0.56	0.43	0.36	0.81	0.51	0.37	0.35	0.37
900	0.77	0.60	0.54	0.40	0.37	*	0.79	0.52	0.43	0.49
1000	0.77	0.67	0.50	0.41	0.40	0.85	0.63	0.43	0.49	0.48
1500	0.82	0.74	0.64	0.60	0.55	1.00	0.52	0.47	0.51	0.62
2000	0.92	0.86	0.75	0.70	0.66	0.82	0.60	0.59	0.65	0.68
1h										
100	*	*	*	*	0.50	*	*	*	*	0.73
200	*	*	0.76	0.39	0.29	*	*	*	0.48	0.33
300	*	*	0.44	0.31	0.25	*	*	*	0.43	0.34
400	*	0.91	0.39	0.27	0.29	*	*	0.56	0.26	0.28
500	*	0.49	0.37	0.27	0.29	*	0.71	0.28	0.25	0.26
600	0.93	0.58	0.37	0.26	0.33	*	0.51	0.25	0.20	0.21
700	0.68	0.57	0.43	0.36	0.41	*	0.28	0.21	0.21	0.25
800	0.56	0.51	0.41	0.38	0.38	1.09	0.26	0.23	0.23	0.28
1i										
100	*	*	*	0.31	0.26	*	0.89	0.66	0.41	0.34
200	*	0.96	0.82	0.33	0.22	*	0.87	0.38	0.21	0.19
300	*	*	0.64	0.38	0.32	*	0.46	0.25	0.18	0.17
400	0.97	0.75	0.51	0.38	0.36	*	0.30	0.19	0.16	0.16
500	0.79	0.66	0.50	0.42	0.43	0.56	0.26	0.19	0.16	0.20
600	0.71	0.66	0.53	0.49	0.49	0.56	0.24	0.20	0.17	0.19
700	0.82	0.70	0.61	0.60	0.64	*	0.28	0.23	0.20	0.21
800	0.84	0.79	0.69	0.66	0.69	0.65	0.29	0.26	0.23	0.21

^aData shown are combination indices. Cal27 and Cal27CisR were treated with combinations of cisplatin and **1g**, **1h**, or **1i**. CI (combination index) was calculated using Calcsyn 2.1 based on the Chou–Talalay method. CI > 1 indicates antagonism, CI = 1 indicates an additive effect, and CI < 0.9 indicates synergism. * means fraction affected is less than 0.20. Values are the mean of three experiments. SD is <10% of the mean.

and **8** in order to understand and explain their selectivity profile. Compounds **1g–i** are the most potent inhibitors of HDAC6 evaluated in this study. All three inhibitors did not produce valid docking poses in HDAC4 and HDAC8 reflecting their high IC₅₀ values toward these isoforms. In contrast, in HDAC1 and -6, binding poses were identified for all three inhibitors similar to the ones found for **1a** (Figure 5). Again, the relative change of the IC₅₀ values of the inhibitors is reflected in the relative change in docking energies (Table 6), with the compounds showing a preference for HDAC6 (Table 5). Moreover, compounds **1g–i** show more favorable docking energies than **1a** in HDAC6 (Table 6), in agreement with the lower IC₅₀ values toward HDAC6 for **1g–i** compared to **1a** (Table 5). The docking results are even sensitive enough to correctly display that **1g** and **1i** exhibit a similar activity toward HDAC6, while **1h** is correctly predicted to be less effective (Table 5, Table 6). The docking poses (Figure 5) suggest that this difference occurs because of the quinoline moiety of **1g** being quite buried in subpocket II, and **1i** filling both subpockets I and II with its methoxy groups; in contrast, the urea oxygen of **1h** is in unfavorably close contact to the protein. Compounds **1g** and **1i** could also form weak hydrogen bonds with C137 at the lower backside of subpocket I, which **1h** cannot form due to the orientation of its quinoline moiety. In all, the results of the docking are in remarkably close agreement with those of the biological evaluation. Furthermore, decoration of the quinoline moiety with small hydrophobic groups resulted in improved binding affinities as hypothesized from the initial

docking studies above. Together with previous successful applications of the combination AutoDock3/DrugScore for ligand docking to HDACs,^{14,16} this corroborates the suitability of these methods for such predictive in silico studies.

Enhancement of Cisplatin-Induced Cytotoxicity. As HDACi are promising new therapeutic agents successfully combined with DNA-damaging compounds such as cisplatin,²³ the ability of **1g–i** to influence the cytotoxic activity (MTT assay) of cisplatin was analyzed. Cal27 and Cal27CisR were preincubated with 1 μ M **1g**, 0.5 μ M **1h**, or 0.5 μ M **1i** 48 h prior to cisplatin administration for another 72 h. IC₅₀ values for cisplatin alone and in combination with **1g–i** are shown in Table 7.

A 48 h preincubation with **1g–i** resulted in a significantly increased cisplatin sensitivity. In the native cell line Cal27, a hypersensitization with shift factors of 6.1 up to 8.7 for cisplatin was observed. This sensitizing effect was also obtained in the cisplatin resistant subline Cal27CisR. With shift factors in the range of 8.2–11.2, the enhancement of cisplatin-induced cytotoxicity was more pronounced in Cal27CisR. IC₅₀ values for cisplatin in Cal27CisR after preincubation with **1g–i** were below the IC₅₀ value of the native cell line Cal27 indicating that **1g–i** are able to overcome cisplatin resistance in the HNSCC cell line Cal27. The HDAC6-selective compound tubastatin A was included as control and only slightly increased cisplatin sensitivity in Cal27CisR (1.5fold) with no effect in native Cal27. This indicates that HDAC6 inhibition may be a minor factor in the in vitro chemosensitizing process and additional

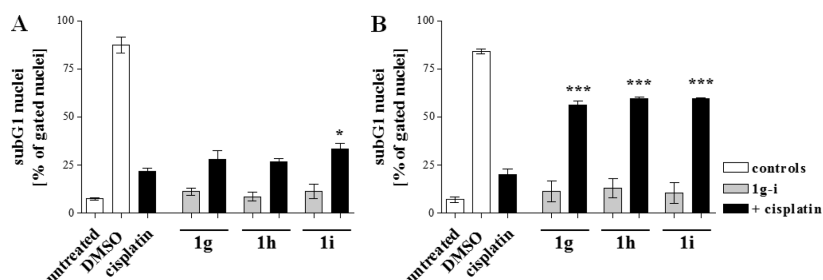


Figure 7. **1g–i** enhance cisplatin-induced apoptosis in Cal27 and Cal27CisR cells. Cal27 (A) and Cal27CisR (B) cells were preincubated with 1 μ M **1g**, 0.5 μ M **1h**, or 0.5 μ M **1i** for 48 h. Cisplatin was added in an IC_{50} concentration for each cell line (Cal27 3 μ M (A), Cal27CisR 25 μ M (B)) and washed out after 6 h. After a further incubation period of 24 h, apoptosis was analyzed by determining the sub-G1 cell fractions by flow cytometry analysis. DMSO 10% was added for 24 h to serve as a positive control for apoptosis induction. Vehicle was added as a control for untreated cells. Gray bars depict the incubation of cells with **1g–i** only, whereas black bars show the effects of the combination of **1g–i** with cisplatin. All experimental conditions were incubated for same time periods. Data are the mean \pm SD, $n = 3$. Statistical analysis to compare the apoptosis induction by cisplatin alone and the combination of cisplatin and **1g–i** was performed using one-way ANOVA test ((*) $p < 0.05$ and (***) $p < 0.001$).

class I HDAC inhibition is required to increase cisplatin sensitivity as seen for vorinostat and **1g–1i**.

Figure 6 shows the effect of the most potent compound **1i** on the inhibitory activity of cisplatin at Cal27CisR cells.

To determine the type of interaction between cisplatin and **1g–i**, we performed synergism studies by using MTT assays. Cal27 and Cal27CisR cells were preincubated with eight different concentrations of **1g–i**. After 48 h, cisplatin was added in five different concentrations and incubated for 72 h similar to the combination experiments shown above. The used concentrations were chosen to achieve a fraction affected (f_a = level of cellular growth inhibition) of <0.9 in the isobologram analysis. Results are shown in Table 8.

With combination indices below 0.9, the isobologram analysis revealed a synergistic effect of **1g–i** with cisplatin. As seen in the combination experiments to analyze an enhancement of cisplatin-induced cytotoxicity, the effects of **1g–i** were more pronounced for the cisplatin-resistant subline. In Cal27CisR, CI values were more than 2-fold lower in comparison to Cal27. These results underline once more the higher efficacy of **1g–i** concerning synergistic cytotoxic effects in the cisplatin resistant subline Cal27CisR.

Enhancement of Cisplatin-Induced Apoptosis. Above, we found a synergistic enhancement of cisplatin-induced cytotoxicity upon a 48 h preincubation with **1g–i**. Here, we evaluated if these results could be due to effects of **1g–i** on cisplatin-induced apoptosis. Cal27 and Cal27CisR cells were treated with 1 μ M **1g** or 0.5 μ M **1h** and **1i** for 48 h. Then, cisplatin was added in a concentration corresponding to the actual IC_{50} for each cell line (Cal27, 3 μ M; Cal27CisR, 25 μ M) and washed out after 6 h. Cells were cultured for another 24 h and analyzed using propidium iodide staining. Results are shown in Figure 7.

1g–i induced no significant changes in the amount of apoptotic nuclei in comparison to the untreated control for both cell lines. This indicates that the concentrations of **1g–i** used for the apoptosis assay and for the combination experiments had no apoptotic effects as single agents. However, in combination with cisplatin **1g–i** induced an increase in apoptosis in comparison to cisplatin alone. The combined treatment in Cal27 showed a significant increase in the amount of apoptotic nuclei for **1i** (33.3% in contrast to 21.8% for cisplatin alone), whereas **1g** and **1h** induced only a small increase which was not significant. In the cell line Cal27CisR, a significant increase in apoptosis induction was observed for all three compounds

(cisplatin, 20.3%; +**1g**, 56.3%; +**1h**, 59.7%; +**1i**, 59.7%) underlining again the higher activity of **1g–i** in the cisplatin-resistant subline.

CONCLUSIONS

In summary, we have developed an improved synthetic protocol for the preparation of HDACi with an alkoxyurea connecting-unit linker region. In particular, compounds **1g–i** showed remarkable inhibition of cellular HDAC activity and cytotoxicity in the human ovarian cancer cell line A2780, the human squamous carcinoma cell line Cal27, and their cisplatin resistant sublines A2780CisR and Cal27CisR. On the basis of their potent anticancer activity, **1g–i** were selected for a comprehensive biological evaluation. Isoform profiling against HDAC1, -4, -6, and -8 resulted in low nanomolar IC_{50} values for HDAC6 with up to 15-fold preference over HDAC1, >3500 -fold over HDAC4, and >100 -fold selectivity over HDAC8. Molecular modeling and docking studies were performed to rationalize the observed selectivity profile. Moreover, our data show that **1g–i** enhanced the cisplatin-induced cytotoxicity in Cal27 and Cal27CisR cells. Notably, **1g–i** interacted synergistically with cisplatin. The enhancement of cisplatin-induced cytotoxicity could be due to an increase in cisplatin-induced apoptosis. These effects are more pronounced in the cisplatin-resistant subline Cal27CisR. These new dual HDAC1/HDAC6 inhibitors may thus be promising modulators to overcome cisplatin resistance in HNSCC.

EXPERIMENTAL SECTION

Chemistry. General. All solvents and chemicals were used as purchased without further purification. The progress of all reactions was monitored on Merck precoated silica gel plates (with fluorescence indicator UV₂₅₄) using ethyl acetate/*n*-hexane as solvent system. Column chromatography was performed with Fluka silica gel 60 (230–400 mesh ASTM) with the solvent mixtures specified in the corresponding experiment. Spots were visualized by irradiation with ultraviolet light (254 nm) or staining in potassium permanganate solution following heating. Flash column chromatography was performed using prepacked silica cartridge with the solvent mixtures specified in the corresponding experiment. Melting points (mp) were taken in open capillaries on a Mettler FP 5 melting-point apparatus and are uncorrected. Proton (¹H) and carbon (¹³C) NMR spectra were recorded on a Bruker Avance 500 (500 MHz for ¹H and 125 MHz for ¹³C) or Bruker Avance 600 (600 MHz for ¹H and 150 MHz for ¹³C) using chloroform-*d* or DMSO-*d*₆ as solvent. Chemical shifts are given in parts per million (ppm), relative to residual solvent peak for ¹H and ¹³C. Elemental analysis was performed on a PerkinElmer PE 2400 CHN elemental analyzer. Analytical HPLC analysis were carried out on a

Varian Prostar system equipped with a Prostar 410 (autosampler), 210 (pumps) and 330 (UV detector) using a Phenomenex Luna Su C18(2) 1.8 μm particle (250 mm \times 4.6 mm) column, supported by Phenomenex Security Guard cartridge kit C18 (4.0 mm \times 3.0 mm). UV absorption was detected at 254 nm with a linear gradient. The purity of all final compounds was 95% or higher.

Experimental Data. General procedures for the synthesis of HDAC inhibitors **1c–j**, **2**, and the *O*-benzyl-protected precursors **6c–j** as well as characterization data for compounds **1i** and **6i** are given below. The synthesis of all other compounds is reported in the [Supporting Information](#).

General Procedure for the Synthesis of Compounds 1c–j, 2. A solution of the respective *O*-benzyl-protected hydroxamic acid (**6c–j**, **9**) in methanol (50 mL) was hydrogenated (1 bar) at room temperature in the presence of a catalytic amount of Pd–C (10 wt %). Upon completion of the reaction, the crude mixture was filtered through Celite to remove the catalyst and the filtrate was concentrated under reduced pressure. The residue was purified by column chromatography using CH_2Cl_2 /30% methanol (9:1) as eluent (yield, 54–72%).

***N*-Hydroxy-6-((3-(naphthalen-2-yl)ureido)oxy)hexanamide (1c).** Colorless solid; yield 65%; mp 195 °C. ^1H NMR (600 MHz, $\text{DMSO}-d_6$) δ = 10.35 (s, 1H), 9.54 (s, 1H), 8.88 (s, 1H), 8.67 (s, 1H), 8.15 (s, 1H), 7.96–7.64 (m, 4H), 7.50–7.33 (m, 2H), 3.80 (t, J = 6.8 Hz, 2H), 1.98 (t, J = 7.6 Hz, 2H), 1.81–1.59 (m, 2H), 1.61–1.48 (m, 2H), 1.42–1.28 (m, 2H) ppm. ^{13}C NMR (151 MHz, $\text{DMSO}-d_6$) δ = 169.0, 157.1, 136.7, 133.4, 129.3, 127.9, 127.3, 126.9, 126.2, 124.1, 120.6, 114.9, 75.7, 32.1, 27.2, 24.9 ppm. HPLC analysis: retention time = 8.13 min; peak area, 96.48%. Method: eluent A, HPLC-grade water + 0.1% TFA; eluent B, HPLC-grade CH_3CN + 0.1% TFA; linear gradient of 30% B to 100% B over 20 min at a flow rate of 1.0 mL min^{-1} .

***N*-Hydroxy-6-((3-(quinolin-6-yl)ureido)oxy)hexanamide (1d).** Colorless solid; yield 62%; mp 153 °C. ^1H NMR (600 MHz, $\text{DMSO}-d_6$) δ = 10.36 (s, 1H), 9.63 (s, 1H), 9.04 (s, 1H), 8.77–8.74 (m, 1H), 8.68 (s, 1H), 8.24 (m, 8.26–8.21, 2H), 7.93 (s, 2H), 7.54–7.36 (m, 1H), 3.80 (t, J = 6.6 Hz, 2H), 1.97 (t, J = 7.4 Hz, 2H), 1.72–1.60 (m, 2H), 1.60–1.47 (m, 2H), 1.40–1.28 (m, 2H) ppm. ^{13}C NMR (151 MHz, $\text{DMSO}-d_6$) δ = 169.0, 157.0, 148.5, 144.3, 137.1, 135.1, 129.0, 128.2, 124.0, 121.5, 114.5, 75.7, 32.1, 27.2, 24.9 ppm. HPLC analysis: retention time = 7.09 min; peak area, 96.33%. Method: eluent A, HPLC-grade water + 0.1% TFA; eluent B, HPLC-grade CH_3CN + 0.1% TFA; linear gradient of 10% B to 100% B over 20 min at a flow rate of 1.0 mL min^{-1} .

***N*-Hydroxy-6-((3-(quinolin-8-yl)ureido)oxy)hexanamide (1e).** Colorless solid; yield 57%; mp 123 °C. ^1H NMR (600 MHz, $\text{DMSO}-d_6$) δ = 10.36 (s, 1H), 9.96 (s, 1H), 9.91 (s, 1H), 8.92–8.87 (m, 1H), 8.67 (s, 1H), 8.48 (d, 1H), 8.41 (d, J = 8.2, 1.7 Hz, 1H), 7.68–7.51 (m, 3H), 3.89 (t, J = 6.3 Hz, 2H), 1.98 (t, J = 7.3 Hz, 2H), 1.76–1.64 (m, 2H), 1.61–1.52 (m, 2H), 1.51–1.42 (m, 2H) ppm. ^{13}C NMR (151 MHz, $\text{DMSO}-d_6$) δ = 169.0, 156.3, 148.8, 137.6, 136.6, 134.4, 127.7, 127.0, 122.1, 120.5, 114.1, 76.0, 32.1, 27.5, 25.1, 24.9 ppm. HPLC analysis: retention time = 9.76 min; peak area, 95.44%. Method: eluent A, HPLC-grade water + 0.1% TFA; eluent B, HPLC-grade CH_3CN + 0.1% TFA; linear gradient of 10% B to 100% B over 20 min at a flow rate of 1.0 mL min^{-1} .

***N*-Hydroxy-6-((3-(2-methylquinolin-8-yl)ureido)oxy)hexanamide (1f).** Colorless solid; yield 72%; mp 153 °C. ^1H NMR (600 MHz, $\text{DMSO}-d_6$) δ = 10.36 (s, 1H), 9.97 (s, 1H), 9.94 (s, 1H), 8.68 (s, 1H), 8.49–8.42 (m, 1H), 8.27 (s, 1H), 7.61–7.40 (m, 3H), 3.91 (t, J = 6.4 Hz, 2H), 2.71 (s, 3H), 2.04–1.93 (m, 2H), 1.85–1.69 (m, 2H), 1.69–1.52 (m, 2H), 1.54–1.41 (m, 2H) ppm. ^{13}C NMR (151 MHz, $\text{DMSO}-d_6$) δ = 168.4, 156.7, 155.9, 136.4, 136.1, 133.3, 125.5, 125.4, 122.2, 119.7, 113.5, 75.6, 31.5, 27.1, 24.5, 24.4, 24.3 ppm. HPLC analysis: retention time = 14.17 min; peak area, 96.99%. Method: eluent A, HPLC-grade water + 0.1% TFA; eluent B, HPLC-grade CH_3CN + 0.1% TFA; linear gradient of 10% B to 100% B over 20 min at a flow rate of 1.0 mL min^{-1} .

***N*-Hydroxy-6-((3-(6-methoxyquinolin-8-yl)ureido)oxy)hexanamide (1g).** Colorless solid; yield 59%; mp 176 °C. ^1H NMR (600 MHz, $\text{DMSO}-d_6$) δ = 10.35 (s, 1H), 10.01 (s, 1H), 9.85 (s, 1H), 8.70 (dd, J = 4.2, 1.6 Hz, 1H), 8.66 (s, 1H), 8.27 (d, J = 8.2 Hz, 1H), 8.14 (d, J = 2.5 Hz, 1H), 7.61–7.52 (m, 1H), 7.01 (d, J = 2.5 Hz, 1H), 3.97–3.82 (m, 5H), 1.98 (t, J = 7.2 Hz, 2H), 1.74–1.64 (m, 2H), 1.61–1.53

(m, 2H), 1.51–1.41 (m, 2H) ppm. ^{13}C NMR (151 MHz, $\text{DMSO}-d_6$) δ = 168.9, 157.6, 156.2, 146.0, 135.4, 135.3, 134.2, 128.9, 122.5, 106.5, 98.5, 76.0, 55.4, 32.1, 27.5, 25.1, 24.9 ppm. HPLC analysis: retention time = 6.88 min; peak area, 95.42%. Method: eluent A, HPLC-grade water + 0.1% TFA; eluent B, HPLC-grade CH_3CN + 0.1% TFA; linear gradient of 30% B to 100% B over 20 min at a flow rate of 1.0 mL min^{-1} .

***N*-Hydroxy-6-((3-(6-methoxy-4-methylquinolin-8-yl)ureido)oxy)hexanamide (1h).** Colorless solid; yield 61%; mp 142 °C. ^1H NMR (600 MHz, $\text{DMSO}-d_6$) δ = 10.36 (s, 1H), 9.99 (s, 1H), 9.95 (s, 1H), 8.67 (s, 1H), 8.56 (dd, J = 4.3, 1.7 Hz, 1H), 8.19–8.11 (m, 1H), 7.42 (d, J = 4.1 Hz, 1H), 6.95 (s, 1H), 3.92 (s, 3H), 3.87 (t, J = 6.4, 1.8 Hz, 2H), 2.65 (s, 3H), 1.98 (t, J = 7.5, 1.7 Hz, 2H), 1.74–1.64 (m, 2H), 1.61–1.53 (m, 2H), 1.50–1.42 (m, 2H) ppm. ^{13}C NMR (125 MHz, $\text{DMSO}-d_6$) δ = 169.0, 157.5, 156.2, 145.5, 143.4, 135.9, 133.9, 128.5, 123.0, 106.0, 95.3, 76.0, 55.4, 32.1, 27.5, 25.1, 24.9, 18.4 ppm. HPLC analysis: retention time = 9.62 min; peak area, 98.50%. Method: eluent A, HPLC-grade water + 0.1% TFA; eluent B, HPLC-grade CH_3CN + 0.1% TFA; linear gradient of 10% B to 100% B over 20 min at a flow rate of 1.0 mL min^{-1} .

6-((3-(2,6-Dimethoxy-4-methylquinolin-8-yl)ureido)oxy)-*N*-hydroxyhexanamide (1i). Colorless solid; yield 55%; mp 162 °C. ^1H NMR (600 MHz, $\text{DMSO}-d_6$) δ = 10.34 (s, 1H), 9.94 (s, 1H), 9.59 (s, 1H), 8.66 (s, 1H), 8.13 (d, 1H), 6.96 (s, 1H), 6.92 (d, J = 2.7 Hz, 1H), 3.98 (s, 3H), 3.95–3.83 (m, 3H), 2.59 (s, 3H), 1.94 (t, J = 7.4 Hz, 2H), 1.70–1.60 (m, 2H), 1.56–1.47 (m, 2H), 1.38–1.29 (m, 2H) ppm. ^{13}C NMR (151 MHz, $\text{DMSO}-d_6$) δ = 168.4, 158.7, 155.8, 155.1, 146.6, 133.6, 130.2, 124.5, 112.5, 105.7, 96.0, 75.3, 54.7, 52.1, 31.6, 27.0, 24.39, 24.32, 17.92 ppm. HPLC analysis: retention time = 14.17 min; peak area, 96.99%. Method: eluent A, HPLC-grade water + 0.1% TFA; eluent B, HPLC-grade CH_3CN + 0.1% TFA; linear gradient of 10% B to 100% B over 20 min at a flow rate of 1.0 mL min^{-1} .

***N*-Hydroxy-6-((3-(2-isopropoxy-6-methoxy-4-methyl-5-(3-(trifluoromethyl)phenoxy)quinolin-8-yl)ureido)oxy)hexanamide (1j).** Colorless solid; yield 54%; mp 137 °C. ^1H NMR (600 MHz, $\text{DMSO}-d_6$) δ = 10.37 (s, 1H), 10.02 (s, 1H), 9.68 (s, 1H), 8.69 (s, 1H), 8.57 (s, 1H), 7.53 (t, J = 8.1, 1H), 7.37 (d, J = 7.8, 1H), 7.12 (s, 1H), 7.03 (d, J = 7.8, 1H), 6.84 (s, 1H), 5.45 (sept, J = 6.2, 1H), 3.91 (t, J = 7.1, 2H), 3.75 (s, 3H), 2.52 (s, 3H), 1.98 (t, J = 7.4, 2H), 1.85–1.63 (m, 2H), 1.63–1.48 (m, 2H), 1.48–1.27 (m, 8H) ppm. ^{13}C NMR (151 MHz, $\text{DMSO}-d_6$) δ = 168.9, 158.7, 158.6, 156.4, 147.4, 146.2, 131.9, 131.1, 130.4 (q, J = 32.0 Hz), 130.4, 130.3, 123.8 (q, J = 272.9 Hz), 119.4, 118.6, 118.2, 116.3, 111.3, 103.7, 75.8, 67.8, 56.3, 32.1, 27.5, 24.9, 24.8, 22.2, 21.6 ppm. HPLC analysis: retention time = 18.61 min; peak area, 96.49%. Method: eluent A, HPLC-grade water + 0.1% TFA; eluent B, HPLC-grade CH_3CN + 0.1% TFA; linear gradient of 30% B to 100% B over 20 min at a flow rate of 1.0 mL min^{-1} .

***N*-(Benzoyloxy)-*N*-methyl-6-((3-(naphthalen-1-yl)ureido)oxy)hexanamide (2).** Oil; yield 54%. ^1H NMR (500 MHz, $\text{DMSO}-d_6$) δ = 9.76 (s, 1H), 9.55 (s, 1H), 8.83 (s, 1H), 8.07–7.87 (m, 2H), 7.75 (d, J = 8.20, 1H), 7.63 (d, J = 7.34, 1H), 7.60–7.46 (m, 3H), 3.88 (t, J = 6.7 Hz, 2H), 3.07 (s, 3H), 2.37 (t, J = 7.7 Hz, 2H), 1.77–1.66 (m, 2H), 1.61–1.49 (m, 2H), 1.47–1.34 (m, 2H) ppm. ^{13}C NMR (125 MHz, $\text{DMSO}-d_6$) δ = 172.8, 157.9, 133.6, 128.3, 128.3, 128.0, 125.8, 125.7, 125.5, 124.8, 122.4, 121.6, 75.8, 35.6, 31.4, 27.4, 25.1, 24.0 ppm. Anal. Calcd for $\text{C}_{18}\text{H}_{23}\text{N}_3$: C 60.51, H 8.07, N 12.45. Found: C 60.58, H 7.93, N 12.15.

***N*-(Benzoyloxy)-6-((1,3-dioxoisindolin-2-yl)oxy)hexanamide (3).** (1) 6-Bromohexanoic acid (1.951 g, 10 mmol) was dissolved in anhydrous THF (25 mL) and cooled to -15 °C. This was treated with *N*-methylmorpholine (1.012 g, 11 mmol) followed by isobutyl chloroformate (1.502 g, 11 mmol) to form the mixed anhydride. After 15 min *O*-benzylhydroxylamine (1.232 g, 10 mmol) was added dropwise. The reaction was warmed to room temperature over 3 h and subsequently filtered. After removing the solvent in vacuo the residue was diluted in ethyl acetate/ H_2O and extracted with ethyl acetate (3 \times 60 mL). The combined extracts were washed with NaHCO_3 (50 mL) and the organic layer was dried over Na_2SO_4 , filtered and the solvent removed in vacuo to give the intermediate *N*-(benzyloxy)-6-bromohexanamide (2.49 g, 8.30 mmol, 83%).

(2) *N*-Hydroxyphthalimide (1.35 g, 8.30 mmol) and *N*-(benzyloxy)-6-bromohexanamide (2.49 g, 8.30 mmol) were dissolved in acetonitrile

(25 mL). Triethylamine (1.26 g, 12.45 mmol) was added, and the reaction mixture was refluxed for 7 h. Upon completion (TLC analysis, eluent ethyl acetate/*n*-hexane 1:1), the reaction mixture was poured into ice–water (70 g) and extracted with ethyl acetate (3 × 75 mL). The combined organic layers were washed with a saturated solution of NaHCO₃ (3 × 75 mL), dried over Na₂SO₄, and evaporated under reduced pressure to provide **3** in 79% yield. All spectroscopic data were in agreement with the literature.¹⁴

6-(Aminoxy)-*N*-(benzyloxy)hexanamide (4). Methylhydrazine (0.503 mL, 9.6 mmol) was added dropwise at –10 °C to a solution of compound **3** (2.29 g, 6 mmol) in dry CH₂Cl₂ (15 mL). The reaction mixture was stirred for 2.5 h, and the precipitate was removed by filtration. The filtrate was evaporated under reduced pressure and treated with diethyl ether (5 mL). The precipitate was removed by filtration, and a saturated solution of HCl in diethyl ether was added to the filtrate to obtain the hydrochloride of the product. The solid was collected by filtration and subsequently dissolved in water (40 mL). A saturated Na₂CO₃ solution was added until pH > 8, and the aqueous layer was extracted with ethyl acetate (3 × 50 mL). The combined organic layers were dried over Na₂SO₄ and evaporated under reduced pressure to provide **4**. All spectroscopic data were in agreement with the literature.¹⁴

4-Nitrophenyl ((6-((benzyloxy)amino)-6-oxohexyl)oxy)carbamate (5). The 6-(aminoxy)-*N*-(benzyloxy)hexanamide **4** (0.252 g, 1.0 mmol) was dissolved in dry CH₂Cl₂ (30 mL), and dry pyridine (0.110 mL, 1.4 mmol) was added. The reaction was cooled down to 0 °C, and 4-nitrophenyl chloroformate (0.202 g, 1 mmol) was added under stirring in one portion. After stirring at room temperature for 3 h, the homogeneous solution was diluted with CH₂Cl₂ (100 mL) and washed with citric acid solution (10% w/w, 2 × 50 mL) and water (2 × 50 mL). The organic layer was dried over Na₂SO₄ and concentrated to afford **5** in 72% yield. Compound **5** was used directly in the next step without further purification.

General Procedure for the Microwave-Assisted Synthesis of Compounds 6c–j. 4-Nitrophenyl-((6-((benzyloxy)amino)-6-oxohexyl)oxy)carbamate **5** (0.209 g, 0.5 mmol) in dry THF (1.5 mL) was placed into a 10 mL glass pressure microwave tube equipped with a magnetic stirrer bar. Triethylamine (69 μL, 0.5 mmol) was added before the tube was closed with a silicon septum, and the reaction mixture was subjected to microwave irradiation for 0.5 h at 70 °C and 100 W. The reaction mixture was cooled to room temperature and transferred to a round bottomed flask. The solvent was evaporated, CH₂Cl₂ (100 mL) was added, and the mixture was washed subsequently with a saturated, aqueous solution of sodium hydrogen carbonate (30 mL), and water (30 mL). The organic layer was dried over Na₂SO₄, filtered, and the solvent was evaporated. The remaining residues were purified by crystallization from appropriate solvents or the crude products were purified by flash column chromatography (prepacked silica cartridge, *n*-hexane/ethyl acetate, gradient 90:10 → 0:100 in 0.5 h) to yield the desired intermediates (yield, 83–91%).

***N*-(Benzyloxy)-6-((3-(naphthalen-2-yl)ureido)oxy)hexanamide (6c).** Colorless solid; yield 85%; mp 132 °C. ¹H NMR (600 MHz, DMSO-*d*₆) δ = 10.96 (s, 1H), 9.54 (s, 1H), 8.87 (s, 1H), 8.15 (d, *J* = 1.6 Hz, 1H), 7.82 (s, 1H), 7.80 (s, 1H), 7.77 (d, *J* = 8.2 Hz, 1H), 7.69 (dd, *J* = 2.0, 8.9 Hz, 1H), 7.44 (t, *J* = 7.5 Hz, 1H), 7.41–7.30 (m, 6H), 4.78 (s, 2H), 3.79 (t, *J* = 6.7 Hz, 2H), 1.98 (t, *J* = 7.2 Hz, 2H), 1.69–1.59 (m, 2H), 1.57–1.48 (m, 2H), 1.37–1.26 (m, 2H) ppm. ¹³C NMR (150 MHz, DMSO-*d*₆) δ = 169.2, 157.1, 136.6, 136.0, 133.3, 129.3, 128.7, 128.2, 128.1, 127.9, 127.3, 126.9, 126.1, 124.1, 120.6, 114.9, 76.7, 75.6, 32.1, 27.2, 24.7, 24.7 ppm. Anal. Calcd for C₂₄H₂₇N₃: C 68.39, H 6.46, N 9.97. Found: C 68.21, H 6.37, N 9.83.

***N*-(Benzyloxy)-6-((3-(quinolin-6-yl)ureido)oxy)hexanamide (6d).** Colorless solid; yield 79%; mp 103 °C. ¹H NMR (600 MHz, DMSO-*d*₆) δ = 10.95 (s, 1H), 9.62 (s, 1H), 9.03 (s, 1H), 8.75 (dd, *J* = 4.0, 1.7 Hz, 1H), 8.26–8.16 (m, 2H), 7.92 (s, 2H), 7.50–7.42 (m, 1H), 7.51–7.27 (m, 5H), 4.78 (s, 2H), 3.80 (t, *J* = 6.7 Hz, 2H), 1.98 (t, *J* = 7.2 Hz, 2H), 1.72–1.60 (m, 2H), 1.59–1.49 (m, 2H), 1.39–1.27 (m, 2H) ppm. ¹³C NMR (151 MHz, DMSO-*d*₆) δ = 169.2, 157.0, 148.5, 144.3, 137.1, 136.0, 135.1, 129.0, 128.7, 128.2, 128.1, 123.9, 121.5, 114.5, 76.7,

75.7, 32.1, 27.1, 24.7, 24.7 ppm. Anal. Calcd for C₂₃H₂₆N₄: C 65.39, H 6.20, N 13.26. Found: C 65.11, H 6.11, N 13.01.

***N*-(Benzyloxy)-6-((3-(quinolin-8-yl)ureido)oxy)hexanamide (6e).** Colorless solid; yield 77%; mp 94 °C. ¹H NMR (600 MHz, DMSO-*d*₆) δ = 10.97 (s, 1H), 9.97 (s, 1H), 9.92 (s, 1H), 8.90 (d, *J* = 2.9 Hz, 1H), 8.49 (d, *J* = 7.5 Hz, 1H), 8.40 (d, *J* = 7.1 Hz, 1H), 7.66–7.52 (m, 3H), 7.43–7.30 (m, 5H), 4.77 (s, 2H), 3.89 (t, *J* = 6.3 Hz, 2H), 2.00 (t, *J* = 7.2 Hz, 2H), 1.74–1.64 (m, 2H), 1.62–1.51 (m, 2H), 1.51–1.42 (m, 2H) ppm. ¹³C NMR (151 MHz, DMSO-*d*₆) δ = 169.2, 156.3, 148.7, 137.6, 136.5, 136.0, 134.4, 128.7, 128.2, 128.1, 127.7, 127.0, 122.1, 120.4, 114.1, 76.7, 76.0, 32.0, 27.4, 24.9, 24.7 ppm. Anal. Calcd for C₂₃H₂₆N₄: C 65.39, H 6.20, N 13.26. Found: C 65.34, H 6.05, N 13.23.

***N*-(Benzyloxy)-6-((3-(2-methylquinolin-8-yl)ureido)oxy)hexanamide (6f).** Colorless solid; yield 89%; mp 110 °C. ¹H NMR (600 MHz, DMSO-*d*₆) δ = 10.93 (s, 1H), 9.96 (s, 1H), 9.93 (s, 1H), 8.44 (dd, *J* = 7.7, 1.4 Hz, 1H), 8.27 (d, *J* = 8.4 Hz, 1H), 7.56–7.44 (m, 3H), 7.39–7.29 (m, 5H), 4.75 (s, 2H), 3.89 (t, *J* = 6.5 Hz, 2H), 2.70 (s, 3H), 1.96 (t, *J* = 7.3 Hz, 2H), 1.78–1.70 (m, 2H), 1.60–1.52 (m, 2H), 1.47–1.39 (m, 2H) ppm. ¹³C NMR (151 MHz, DMSO-*d*₆) δ = 168.7, 156.7, 155.9, 136.4, 136.1, 135.5, 133.3, 128.2, 127.7, 127.6, 125.5, 125.4, 122.2, 119.7, 113.5, 76.1, 75.5, 31.5, 27.0, 24.4, 24.3, 24.2 ppm. Anal. Calcd for C₂₄H₂₈N₄: C 66.04, H 6.47, N 12.84. Found: C 66.07, H 6.33, N 12.77.

***N*-(Benzyloxy)-6-((3-(6-methoxyquinolin-8-yl)ureido)oxy)hexanamide (6g).** Colorless solid; yield 91%; mp 102 °C. ¹H NMR (600 MHz, DMSO-*d*₆) δ = 10.96 (s, 1H), 10.02 (s, 1H), 9.86 (s, 1H), 8.75–8.66 (m, 1H), 8.27 (dd, *J* = 8.3, 1.7 Hz, 1H), 8.15 (d, *J* = 2.8 Hz, 1H), 7.59–7.52 (m, 1H), 7.41–7.31 (m, 5H), 7.01 (d, *J* = 2.8 Hz, 1H), 4.78 (s, 2H), 3.96–3.81 (m, 5H), 2.00 (t, *J* = 7.5 Hz, 2H), 1.76–1.64 (m, 2H), 1.64–1.52 (m, 2H), 1.53–1.41 (m, 2H) ppm. ¹³C NMR (151 MHz, DMSO-*d*₆) δ = 169.2, 157.6, 156.2, 146.0, 136.0, 135.4, 135.3, 134.2, 128.9, 128.7, 128.2, 128.1, 122.5, 106.5, 98.5, 76.7, 76.0, 55.4, 32.0, 27.4, 24.9, 24.7 ppm. Anal. Calcd for C₂₄H₂₈N₄: C 63.70, H 6.24, N 12.38. Found: C 63.41, H 6.09, N 12.23.

***N*-(Benzyloxy)-6-((3-(6-methoxy-4-methylquinolin-8-yl)ureido)oxy)hexanamide (6h).** Colorless solid; yield 78%; mp 110 °C. ¹H NMR (600 MHz, DMSO-*d*₆) δ = 10.95 (s, 1H), 9.99 (s, 1H), 9.95 (s, 1H), 8.56 (d, *J* = 4.2 Hz, 1H), 8.15 (d, *J* = 2.6 Hz, 1H), 7.50–7.26 (m, 6H), 6.95 (d, *J* = 2.6 Hz, 1H), 4.76 (s, 2H), 3.91 (s, 3H), 3.86 (t, *J* = 6.3 Hz, 2H), 2.65 (s, 3H), 1.98 (t, *J* = 6.2 Hz, 2H), 1.75–1.62 (m, 2H), 1.61–1.51 (m, 2H), 1.51–1.40 (m, 2H) ppm. ¹³C NMR (151 MHz, DMSO-*d*₆) δ = 169.2, 157.5, 156.2, 145.5, 143.4, 136.0, 135.8, 133.8, 128.7, 128.5, 128.2, 128.1, 123.0, 106.0, 95.2, 76.6, 76.0, 55.4, 32.0, 27.4, 24.9, 24.7, 18.4 ppm. Anal. Calcd for C₂₅H₃₀N₄: C 64.36, H 6.48, N 12.01. Found: C 64.13, H 6.43, N 12.15.

***N*-(Benzyloxy)-6-((3-(2,6-dimethoxy-4-methylquinolin-8-yl)ureido)oxy)hexanamide (6i).** Colorless solid; yield 84%; mp 132 °C. ¹H NMR (600 MHz, DMSO-*d*₆) δ = 10.95 (s, 1H), 9.94 (s, 1H), 9.58 (s, 1H), 8.13 (d, *J* = 2.7 Hz, 1H), 7.42–7.30 (m, 5H), 6.93 (s, 1H), 6.90 (d, *J* = 2.8 Hz, 1H), 4.77 (s, 2H), 3.98 (s, 3H), 3.88 (m, 3.91–3.85, 5H), 2.57 (s, 3H), 1.96 (t, *J* = 7.3 Hz, 2H), 1.69–1.61 (m, 2H), 1.56–1.48 (m, 2H), 1.37–1.28 (m, 2H) ppm. ¹³C NMR (151 MHz, DMSO-*d*₆) δ = 169.1, 159.2, 156.3, 155.7, 147.2, 136.0, 134.1, 130.7, 128.7, 128.2, 128.1, 125.0, 113.0, 106.2, 96.5, 76.7, 75.8, 55.2, 52.6, 32.0, 27.5, 24.7, 18.4 ppm. Anal. Calcd for C₂₆H₃₂N₄: C 62.89, H 6.50, N 11.28. Found: C 62.67, H 6.44, N 11.03.

***N*-(Benzyloxy)-6-((3-(2-isopropoxy-6-methoxy-4-methyl-5-(3-(trifluoromethyl)phenoxy)quinolin-8-yl)ureido)oxy)hexanamide (6j).** Colorless solid; yield 83%; mp 109 °C. ¹H NMR (600 MHz, DMSO-*d*₆) δ = 10.95 (s, 1H), 10.01 (s, 1H), 9.67 (s, 1H), 8.56 (s, 1H), 7.52 (t, *J* = 8.1 Hz, 1H), 7.45–7.25 (m, 6H), 7.11 (s, 1H), 7.03 (dd, *J* = 8.5, 2.6 Hz, 1H), 6.84 (s, 1H), 5.44 (sept, *J* = 6.2 Hz, 1H), 4.78 (s, 2H), 3.90 (t, *J* = 6.9 Hz, 2H), 3.74 (s, 3H), 2.52 (s, 3H), 1.98 (t, *J* = 7.2 Hz, 2H), 1.73–1.64 (m, 2H), 1.62–1.47 (m, 2H), 1.39 (d, *J* = 9.5 Hz, 6H), 1.37–1.30 (m, 2H) ppm. ¹³C NMR (151 MHz, DMSO-*d*₆) δ = 169.2, 158.7, 158.6, 156.4, 147.4, 146.2, 136.1, 132.0, 131.1, 131.1, 130.4 (q, *J* = 31.93 Hz), 130.4, 128.7, 128.2, 128.1, 123.8 (q, *J* = 272.79 Hz), 119.4, 118.6, 118.2, 116.3, 111.3, 103.7, 76.7, 75.8, 67.8, 56.3, 32.1, 27.5, 24.7, 24.7, 22.2, 21.6 ppm. Anal. Calcd for C₃₅H₃₉N₄: C 61.40, H 5.74, N 8.18. Found: C 61.21, H 5.68, N 8.03.

***N*-(Benzyloxy)-6-((1,3-dioxoisindolin-2-yl)oxy)-*N*-methylhexanamide (7).** Sodium hydride (0.52 g, 13.4 mmol, 60% dispersion in mineral oil) was added in portions to 4.59 g (12 mmol) of *N*-(benzyloxy)-6-((1,3-dioxoisindolin-2-yl)oxy)hexanamide (3) in 115 mL of THF followed by dropwise addition of methyl iodide (0.84 mL, 13.4 mmol). The reaction was stirred overnight at room temperature before it was quenched with a saturated solution of NH₄Cl (100 mL) and extracted with ethyl acetate (3 × 100 mL). The organic layer was dried over Na₂SO₄, filtered, and the solvent was removed in vacuo. The crude products were purified by flash column chromatography (prepacked silica cartridge, *n*-hexane/ethyl acetate, gradient 90:10 → 50:50 in 0.5 h) to give the intermediate *N*-(benzyloxy)-6-((1,3-dioxoisindolin-2-yl)oxy)-*N*-methylhexanamide 7 in 92% yield.²⁵

***N*-(Benzyloxy)-6-((1,3-dioxoisindolin-2-yl)oxy)-*N*-methylhexanamide (7).** Oil; yield 59%. ¹H NMR (500 MHz, DMSO-*d*₆) δ = 7.86 (s, 4H), 7.52–7.30 (m, 5H), 4.89 (s, 2H), 4.11 (t, *J* = 6.5 Hz, 2H), 3.14 (s, 3H), 2.34 (t, *J* = 7.3 Hz, 2H), 1.71–1.58 (m, 2H), 1.57–1.44 (m, 2H), 1.44–1.34 (m, 2H) ppm. ¹³C NMR (125 MHz, DMSO-*d*₆) δ = 163.2, 134.6, 129.4, 128.6, 128.5, 128.4, 123.1, 77.5, 75.1, 31.1, 31.1, 27.4, 24.8, 23.6 ppm. HPLC analysis: retention time = 3.1 min; peak area, 95.34%. Method: eluent A, 5 mM/L (385 mg/L) ammonium acetate; eluent B, HPLC-grade CH₃CN; linear gradient of 5% B to 95% B over 20 min at a flow rate of 1.0 mL min⁻¹.

6-(Aminoxy)-*N*-(benzyloxy)-*N*-methylhexanamide (8). Synthesized from 7 according to the procedure for 4.¹⁴ Oil; yield 62%. ¹H NMR (500 MHz, DMSO-*d*₆) δ = 7.54–7.30 (m, 5H), 5.86 (s, 2H), 4.87 (s, 2H), 3.47 (t, *J* = 6.5 Hz, 2H), 3.13 (s, 3H), 2.30 (t, *J* = 7.5 Hz, 2H), 1.60–1.36 (m, 4H), 1.31–1.13 (m, 2H). ¹³C NMR (151 MHz, DMSO-*d*₆) δ = 173.7, 134.8, 129.4, 128.6, 128.4, 75.1, 74.7, 32.7, 31.2, 27.7, 25.3, 23.9 ppm. Anal. Calcd for C₁₄H₂₂N₂O: C 63.13, H 8.33, N 10.52. Found: C 63.11, H 8.60, N 10.39.

***N*-(Benzyloxy)-*N*-methyl-6-(3-naphthalen-1-ylureidooxy)hexanamide (9).** Synthesized from 8 according to the literature.¹⁴ A solution of 1-naphthyl isocyanate (2.7 mmol) in dry CH₂Cl₂ (5 mL) was added dropwise to a solution of the aminoxy derivative 8 (3 mmol) in dry CH₂Cl₂ (15 mL). The reaction mixture was stirred overnight at room temperature and subsequently treated with petroleum ether to precipitate the product. The resulting solid was collected, washed with petroleum ether (5 mL), and dried in vacuo.

***N*-(Benzyloxy)-*N*-methyl-6-(3-naphthalen-1-ylureidooxy)hexanamide (9).** Oil; yield 59%. ¹H NMR (500 MHz, DMSO-*d*₆) δ = 9.55 (s, 1H), 8.82 (s, 1H), 7.95–7.91 (m, 2H), 7.75 (d, *J* = 8.18, 1H), 7.63 (d, *J* = 7.20 Hz, 1H), 7.57–7.34 (m, 8H), 4.87 (s, 2H), 3.86 (t, *J* = 6.69, 2H), 3.12 (s, 3H), 2.35 (t, *J* = 7.37 Hz, 2H), 1.71–1.61 (m, 2H), 1.78–1.70 (m, 2H), 1.56–1.44 (m, 2H), 1.34–1.25 (m, 2H) ppm. ¹³C NMR (151 MHz, DMSO-*d*₆) δ = 170.2, 157.9, 134.8, 133.6, 133.6, 129.4, 128.6, 128.4, 128.3, 128.0, 125.8, 125.7, 125.5, 124.7, 122.3, 121.6, 75.7, 75.0, 31.2, 27.4, 25.0, 23.8 ppm. Anal. Calcd for C₂₅H₂₉N₃O: C 68.95, H 6.71, N 9.65. Found: C 68.75, H 6.89, N 9.20.

Amine Precursors. The amine intermediates and their precursors were synthesized according to established literature methods or were obtained from commercial suppliers. 2-Naphthylamine, 6-aminoquinoline, 8-aminoquinoline, and 2-methyl-8-nitroquinoline were obtained from commercial suppliers (Sigma-Aldrich, TCI, Alfa Aesar) and used as purchased without further purification. 8-Amino-2-methylquinoline was synthesized from 2-methyl-8-nitroquinoline.²⁶ The known intermediates 6-methoxy-4-methylquinolin-8-amine, 6-methoxyquinolin-8-amine, and 2,6-dimethoxy-4-methylquinolin-8-amine and their precursors were synthesized according to established literature methods.²⁶ The novel 2-isopropoxy-6-methoxy-4-methyl-5-(3-(trifluoromethyl)phenoxy)quinolin-8-amine was synthesized according to known procedures.²⁶

2-Isopropoxy-6-methoxy-4-methyl-8-nitro-5-(3-(trifluoromethyl)phenoxy)quinoline. A solution of the respective phenol (16.3 mmol) in DMSO (15 mL) and potassium hydroxide (0.92 g, 16.3 mmol) was heated to 100 °C for 0.5 h. The respective 2-alkoxy-5-chloro-6-methoxy-4-methyl-8-nitroquinoline (14.2 mmol) was added in one portion. The resulting dark solution was stirred at 100 °C for 2.5 h. Water (30 mL) was added slowly while keeping the temperature above 60 °C. The resulting suspension was cooled to 10 °C. The crude product

was separated by suction filtration, washed with water, and dried. The residue was then suspended in toluene (125 mL), heated to reflux in the presence of activated charcoal, and filtered through kieselgur. Toluene (100 mL) was removed by distillation at ambient pressure. The solution was cooled to 70 °C, and *n*-hexane was added (100 mL). The resulting suspension was cooled to 5 °C. The product was separated by suction filtration and washed with *n*-hexane.

2-Isopropoxy-6-methoxy-4-methyl-8-nitro-5-(3-(trifluoromethyl)phenoxy)quinoline. Yellow solid; yield 64%; mp 155 °C. ¹H NMR (500 MHz, CDCl₃) δ = 7.75 (s, 1H), 7.40 (dd, *J*₁ = *J*₂ = 8.0 Hz, 1H), 7.32 (d, *J* = 7.7 Hz, 1H), 7.09 (s, 1H), 6.93 (d, *J* = 8.2 Hz, 1H), 6.72 (s, 1H), 5.41 (sept, *J* = 6.2 Hz, 1H), 3.80 (s, 3H), 2.61 (s, 3H), 1.39 (d, *J* = 6.2 Hz, 6H) ppm. ¹³C NMR (125 MHz, CDCl₃) δ = 161.7, 157.9, 146.2, 145.8, 144.4, 140.8, 135.2, 132.3 (q, *J* = 32.7 Hz), 130.4, 123.7 (q, *J* = 273.2 Hz), 121.7, 119.2 (q, *J* = 3.6 Hz), 118.2, 118.0, 112.2 (q, *J* = 3.5 Hz), 111.2, 69.4, 57.0, 23.1, 21.8. Anal. Calcd for C₂₁H₁₉F₃N₂O₅: C 57.80, H 4.39, N 6.42. Found: C 57.65, H 4.66, N 6.45.

2-Isopropoxy-6-methoxy-4-methyl-5-(3-(trifluoromethyl)phenoxy)quinoline-8-amine. The respective 8-nitroquinoline (3.7 mmol) and Pd–C (10%) were suspended in dry ethanol (50 mL). The reaction mixture was heated to 60 °C, and then hydrazine hydrate (0.93 g, 18.5 mmol) was added dropwise over 15 min. The reaction mixture was stirred at 60 °C for 4 h, then heated under reflux for 0.5 h. After cooling to 50 °C, Pd–C was removed by filtration through kieselgur and washed with ethanol (20 mL). After cooling to room temperature, water (50 mL) was added slowly under vigorous stirring over 0.5 h. The resulting slurry was cooled to 5 °C, filtered, and the residue was washed with a mixture of ethanol/H₂O (1:1).

2-Isopropoxy-6-methoxy-4-methyl-5-(3-(trifluoromethyl)phenoxy)quinoline-8-amine. Colorless solid; yield 44%; mp 91 °C. ¹H NMR (500 MHz, CDCl₃) δ = 7.33 (dd, *J*₁ = *J*₂ = 8.0 Hz, 1H), 7.21 (d, *J* = 7.7 Hz, 1H), 7.05 (s, 1H), 6.94 (dd, *J* = 8.2, 2.0 Hz, 1H), 6.77 (s, 1H), 6.61 (s, 1H), 5.46 (sept, *J* = 6.2 Hz, 1H), 4.69 (s, 2H), 3.75 (s, 3H), 2.54 (s, 3H), 1.41 (d, *J* = 6.2 Hz, 6H) ppm. ¹³C NMR (126 MHz, CDCl₃) δ = 159.6, 158.9, 148.2, 146.0, 141.1, 131.9 (q, *J* = 32.6 Hz), 131.3, 130.0, 128.6, 123.9 (q, *J* = 272.3 Hz), 120.6, 118.2, 118.0 (q, *J* = 3.8 Hz), 116.4, 112.0 (q, *J* = 3.7 Hz), 99.3, 67.8, 56.7, 23.0, 22.0 ppm. Anal. Calcd for C₂₁H₂₁F₃N₂O₃: C 62.06, H 5.21, N 6.89. Found: C 62.01, H 5.60, N 6.80.

Molecular Modeling. Docking Studies. For the molecular docking, compounds 1a, 1g, 1h, and 1i were drawn with ChemDraw Ultra,²⁷ converted into a 3D structure, and energy minimized with Moloc using the MAB force field.²⁸ The HDACi were then docked into crystal structures of HDAC1 (PDB code 4BKX²⁹), HDAC4 (PDB code 4CBT³⁰), and HDAC8 (PDB code 4RN0³¹) and into a homology model of HDAC6, which was already successfully used by us to predict HDACi binding mode models,¹⁶ utilizing AutoDock3³² as a docking engine and the DrugScore³³ distance-dependent pair-potentials as an objective function, as described in ref 20. In the docking, default parameters were used with the exception of the clustering rmsd cutoff, which was set to 2.0 Å, to consider the flexibly connected saturated and unsaturated carbon cycles. Docking solutions with more than 20% of all configurations in the largest cluster were considered sufficiently converged. The configuration in the largest cluster with the lowest docking energy and with a distance of <3 Å between the hydroxamic acid oxygen and the zinc ion in the binding pocket was used for further evaluation.

Biological Evaluation. Reagents. Cisplatin was purchased from Sigma (Germany), propidium iodide (PI) was purchased from Santa Cruz Biotechnology (Germany), and tubastatin A and entinostat were purchased from Selleckchem (Germany). Vorinostat was synthesized according to known procedures.³⁴ All other reagents were supplied by PAN Biotech (Germany) unless otherwise stated.

Cell Lines and Cell Culture. The human ovarian carcinoma cell line A2780 was obtained from European Collection of Cell Cultures (ECACC, Salisbury, U.K.). The human tongue cell line Cal27 was obtained from the German Collection of Microorganisms and Cell Cultures (DSMZ, Germany). The corresponding cisplatin resistant CisR cell lines were generated by exposing the parental cell lines to

weekly cycles of cisplatin in an IC_{50} concentration over a period of 24–30 weeks as described in Gosepath et al.³⁵ and Eckstein et al.³⁶ The human medulloblastoma cell lines ONS76 and Med8a were a kind gift of the KMT laboratory (Department of Pediatric Oncology, Hematology and Clinical Immunology, Heinrich Heine University Düsseldorf, Germany).

All cell lines were grown at 37 °C under humidified air supplemented with 5% CO_2 in RPMI 1640 (A2780) or DMEM (Cal27, ONS76, Med8a) containing 10% fetal calf serum, 120 IU/mL penicillin, and 120 μ g/mL streptomycin. The cells were grown to 80% confluency before using them for the appropriate assays.

In Vitro Testing of HDAC1, -6, and -8.³⁷ OptiPlate-96 black microplates (PerkinElmer) were used with an assay volume of 60 μ L. Human recombinant HDAC1 (BPS Bioscience, catalog no. 50051) or human recombinant HDAC6 (BPS Bioscience, catalog no. 50006) was diluted in incubation buffer (50 mM Tris-HCl, pH 8.0, 137 mM NaCl, 2.7 mM KCl, 1 mM $MgCl_2$, and 1 mg/mL BSA). An amount of 52 μ L of this dilution was incubated with 3 μ L of different concentrations of inhibitors in DMSO and 5 μ L of the fluorogenic substrate ZMAL (Z-(Ac)Lys-AMC)³⁸ (126 μ M) at 37 °C. After a 90 min incubation time 60 μ L of the stop solution (33 μ M trichostatin A (TSA) and 6 mg/mL trypsin in trypsin buffer (Tris-HCl 50 mM, pH 8.0, NaCl 100 mM)) were added. After a following incubation at 37 °C for 30 min, the fluorescence was measured on a BMG LabTech POLARstar OPTIMA plate reader (BMG LabTech, Germany) with an excitation wavelength of 390 nm and an emission wavelength of 460 nm. For the inhibition of human HDAC8 1/2-AREAPLATE-96 F microplates (PerkinElmer) with an assay volume of 30 μ L were used. Human HDAC8 enzyme was obtained as described before.³⁹ An amount of 22.5 μ L of enzyme diluted in incubation buffer (50 mM KH_2PO_4 , 15 mM Tris, pH 7.5, 3 mM $MgSO_4 \cdot 7 H_2O$, 10 mM KCl) was mixed with 2.5 μ L of inhibitor in DMSO and 5 μ L of Z-L-Lys(ϵ -trifluoroacetyl)-AMC (150 μ M). The plate was incubated at 37 °C for 90 min. An amount of 30 μ L of the stop solution (see HDAC1 and HDAC6) was added, and the plate was incubated again at 37 °C for 30 min. Measurement was performed as described for HDAC1/6.

In Vitro Testing of HDAC4. The in vitro inhibitory activity of compounds **1a** and **1g–i** against HDAC4 isoform was performed at Reaction Biology Corp. (Malvern, PA) with a fluorescent based assay according to the company's standard operating procedure. The IC_{50} values were determined using 10 different concentrations with 3-fold serial dilution. TMP269 was used as reference compound.

MTT Cell Viability Assay. The rate of cell survival under the action of test substances was evaluated by an improved MTT assay as previously described.^{14,40} The assay is based on the ability of viable cells to metabolize yellow 3-(4,5-dimethylthiazol-2-yl)-2,5-diphenyltetrazolium bromide (MTT, Serva, Germany) to violet formazan that can be detected spectrophotometrically. In brief, A2780 and Cal27 cell lines were seeded at a density of 5000 and 2500 cells/well in 96-well plates (Corning, Germany). After 24 h, cells were exposed to increased concentrations of the test compounds. Incubation was ended after 72 h, and cell survival was determined by addition of MTT solution (5 mg/mL in phosphate buffered saline). The formazan precipitate was dissolved in DMSO (VWR, Germany). Absorbance was measured at 544 and 690 nm in a FLUOstar microplate reader (BMG LabTech, Offenburg, Germany).

CellTiter-Glo Luminescent Cell Viability Assay. ONS76 and Med8a were seeded at a density of 1000 and 2000 cells/well in 384-well plates (Corning) and incubated with increasing concentrations of the test compounds. After 72 h the Celltiter Glo reagent was added, and after shaking the plates for 2 min and a subsequent incubation time of 10 min the luminescent signals were read on a Spark 10M microplate reader (Tecan).

Combination Experiments. For the investigation of the effect of **1g–i** on cisplatin induced cytotoxicity, the compounds were added 48 h before cisplatin administration. After 72 h, the cytotoxic effect was determined with a MTT cell viability assay. Calcsyn software 2.1 (Biosoft, U.K.) was used to calculate the combination index (CI) as a quantitative measure of the degree of drug interactions.

Whole-Cell HDAC Inhibition Assay. The cellular HDAC assay was based on an assay published by Ciossek et al.⁴¹ and Bonfils et al.⁴² with minor modifications as described in ref 14. Briefly, human cancer cell lines Cal27/Cal27CisR and A2780/A2780CisR were seeded in 96-well tissue culture plates (Corning, Germany) at a density of 1.5×10^4 cells/well in a total volume of 90 μ L of culture medium. After 24 h, cells were incubated for 18 h with increasing concentrations of test compounds. The reaction was started by adding 10 μ L of 3 mM Boc-Lys(ϵ -Ac)-AMC (Bachem, Germany) to reach a final concentration of 0.3 mM.⁴³ The cells were incubated with the Boc-Lys(ϵ -Ac)-AMC for 3 h under cell culture conditions. After this incubation, 100 μ L/well stop solution (25 mM Tris-HCl (pH 8), 137 mM NaCl, 2.7 mM KCl, 1 mM $MgCl_2$, 1% NP40, 2.0 mg/mL trypsin, 10 μ M vorinostat) was added and the reaction was developed for 3 h under cell culture conditions. Fluorescence intensity was measured at excitation of 320 nm and emission of 520 nm in a NOVOstar microplate reader (BMG LabTech, Offenburg, Germany).

Measurement of Apoptotic Cells. Cal27 and Cal27CisR cells were seeded at a density of 3×10^5 cells/well in 24-well plates (Sarstedt, Germany). Cells were treated with **1g–i** and cDDP alone or in combination for the indicated time points. Supernatant was removed after a centrifugation step, and the cells were lysed in 500 μ L of hypotonic lysis buffer (0.1% sodium citrate, 0.1% Triton X-100, 100 μ g/mL PI) at 4 °C in the dark overnight. The percentage of apoptotic nuclei with DNA content in sub-G1 was analyzed by flow cytometry using the CyFlow instrument (Partec, Germany).

Immunoblotting. Cells were treated with 1 μ M **1g–i** or vehicle for 24 h. The pan-HDACi vorinostat and the HDAC1 and -3 selective inhibitor entinostat were used as controls. Cell pellets were dissolved with lysis buffer 6 (Bio-Techne, Germany) and clarified by centrifugation. Equal amounts of total protein (20 μ g) were resolved by SDS-PAGE and transferred to polyvinylidene fluoride membranes. Blots were incubated with primary antibodies against acetylated α -tubulin, α -tubulin, and acetyl histone H3 (Lys24) (Santa Cruz Biotechnology, Germany). Immunoreactive proteins were visualized using luminol reagent (Santa Cruz Biotechnology, Heidelberg, Germany) with an Intas imager (Intas, Germany). Densitometric analysis was performed on scanned images using the ImageJ software (National Institutes of Health).⁴⁴

Data Analysis. Concentration–effect curves were constructed with Prism 4.0 (GraphPad, San Diego, CA) by fitting the pooled data of at least three experiments performed in triplicates to the four-parameter logistic equation. Statistical analysis was performed using *t* test or one-way ANOVA.

■ ASSOCIATED CONTENT

📄 Supporting Information

The Supporting Information is available free of charge on the ACS Publications website at DOI: 10.1021/acs.jmedchem.6b01538.

Coordinates information for structure representation (PDB)

Molecular formula strings and some data (CSV)

Characterization data of compounds **1c–j** and **6c–j** and of the precursors and general procedures (PDF)

■ AUTHOR INFORMATION

Corresponding Authors

*M.U.K.: phone, +49 211 81-14587; fax, +49 211 81-13847; e-mail, Matthias.kassack@uni-duesseldorf.de.

*T.K.: phone, +49 211 81-14984; fax, +49 211 81-13847; e-mail, Thomas.kurz@uni-duesseldorf.de.

ORCID

Finn K. Hansen: 0000-0001-9765-5975

Manfred Jung: 0000-0002-6361-7716

Holger Gohlke: 0000-0001-8613-1447

Thomas Kurz: 0000-0002-9474-4224

Author Contributions

○K.S. and A.H. contributed equally to this work.

Author Contributions

◆M.U.K. and T.K. share the senior authorship.

Notes

The authors declare no competing financial interest.

†L.M. passed away on October 20, 2011.

Authors will release the atomic coordinates and experimental data upon article publication.

ACKNOWLEDGMENTS

The authors thank the COST Action CM1406 (Epigenetic Chemical Biology EPICHEMbio) for support. J.S. and M.J. thank the Deutsche Forschungsgemeinschaft (DFG, Grant Ju295/13-1) for funding. V.M. thanks the Duesseldorf School of Oncology (funded by the Comprehensive Cancer Center Dusseldorf/Deutsche Krebshilfe and the Medical Faculty HHU Duesseldorf) for funding. This work was supported by institutional funds from the Centre National de la Recherche Scientifique (CNRS), the Institute National de la Santé et de la Recherche Médicale (INSERM), and the Université de Strasbourg. The Deutsche Forschungsgemeinschaft (DFG) is acknowledged for funds used to purchase the UHR-TOF maXis 4G, Bruker Daltonics, Bremen HRMS instrument used in this research.

ABBREVIATIONS USED

CisR, cisplatin resistant subclone; HDAC, histone deacetylase; HDACi, histone deacetylase inhibitors; MTT, 3-(4,5-dimethylthiazol-2-yl)-2,5-diphenyltetrazolium bromide; Pd/C, palladium on activated carbon; rt, room temperature; THF, tetrahydrofuran

REFERENCES

- (1) Falkenberg, K. J.; Johnstone, R. W. Histone deacetylases and their inhibitors in cancer, neurological diseases and immune disorders. *Nat. Rev. Drug Discovery* **2014**, *13*, 673–691.
- (2) Seto, E.; Yoshida, M. Erasers of histone acetylation: the histone deacetylase enzymes. *Cold Spring Harbor Perspect. Biol.* **2014**, *6*, a018713.
- (3) (a) Wagner, J. M.; Hackanson, B.; Lubbert, M.; Jung, M. Histone deacetylase (HDAC) inhibitors in recent clinical trials for cancer therapy. *Clin. Epigenet.* **2010**, *1*, 117–136. (b) Keller, K.; Jung, M. Histone deacetylase (HDAC) inhibitors in recent clinical trials for cancer therapy. In *Epigenetic Therapy of Cancer Preclinical Models and Treatment Approaches*, 1st ed.; Lübbert, M., Jones, P. A., Eds.; Springer-Verlag: Berlin, 2014; pp 227–255, DOI: 10.1007/978-3-642-38404-2_10.
- (4) (a) Prince, H. M.; Bishton, M. J.; Johnstone, R. W. Panobinostat (LBH589): a potent pan-deacetylase inhibitor with promising activity against hematologic and solid tumors. *Future Oncol.* **2009**, *5*, 601–612. (b) Garnock-Jones, K. P. Panobinostat: first global approval. *Drugs* **2015**, *75*, 695–704.
- (5) Shi, Y.; Dong, M.; Hong, X.; Zhang, W.; Feng, J.; Zhu, J.; Yu, L.; Ke, X.; Huang, H.; Shen, Z.; Fan, Y.; Li, W.; Zhao, X.; Qi, J.; Huang, H.; Zhou, D.; Ning, Z.; Lu, X. Results from a multicenter, open-label, pivotal phase II study of chidamide in relapsed or refractory peripheral T-cell lymphoma. *Ann. Oncol.* **2015**, *26*, 1766–1771.
- (6) (a) Rasmussen, T. A.; Schmeltz Sogaard, O.; Brinkmann, C.; Wightman, F.; Lewin, S. R.; Melchjorsen, J.; Dinarello, C.; Ostergaard, L.; Tolstrup, M. Comparison of HDAC inhibitors in clinical development: effect on HIV production in latently infected cells and T-cell activation. *Hum. Vaccines Immunother.* **2013**, *9*, 993–1001.

(b) Azzi, A.; Cosseau, C.; Grunau, C. Schistosoma mansoni: developmental arrest of miracidia treated with histone deacetylase inhibitors. *Exp. Parasitol.* **2009**, *121*, 288–291. (c) Hansen, F. K.; Skinner-Adams, T. S.; Duffy, S.; Marek, L.; Sumanadasa, S. D.; Kuna, K.; Held, J.; Avery, V. M.; Andrews, K. T.; Kurz, T. Synthesis, antimalarial properties, and SAR studies of alkoxyurea-based HDAC inhibitors. *ChemMedChem* **2014**, *9*, 665–670. (d) Hansen, F. K.; Sumanadasa, S. D.; Stenzel, K.; Duffy, S.; Meister, S.; Marek, L.; Schmetter, R.; Kuna, K.; Hamacher, A.; Mordmuller, B.; Kassack, M. U.; Winzeler, E. A.; Avery, V. M.; Andrews, K. T.; Kurz, T. Discovery of HDAC inhibitors with potent activity against multiple malaria parasite life cycle stages. *Eur. J. Med. Chem.* **2014**, *82*, 204–213. (e) Trenholme, K.; Marek, L.; Duffy, S.; Pradel, G.; Fisher, G.; Hansen, F. K.; Skinner-Adams, T. S.; Butterworth, A.; Ngwa, C. J.; Moecking, J.; Goodman, C. D.; McFadden, G. I.; Sumanadasa, S. D.; Fairlie, D. P.; Avery, V. M.; Kurz, T.; Andrews, K. T. Lysine acetylation in sexual stage malaria parasites is a target for antimalarial small molecules. *Antimicrob. Agents Chemother.* **2014**, *58*, 3666–3678.

(7) Micelli, C.; Rastelli, G. Histone deacetylases: structural determinants of inhibitor selectivity. *Drug Discovery Today* **2015**, *20*, 718–735.

(8) Kim, K. P.; Park, S. J.; Kim, J. E.; Hong, Y. S.; Lee, J. L.; Bae, K. S.; Cha, H.; Kwon, S. K.; Ro, S.; Cho, J.; Kim, T. W. First-in-human study of the toxicity, pharmacokinetics, and pharmacodynamics of CG200745, a pan-HDAC inhibitor, in patients with refractory solid malignancies. *Invest. New Drugs* **2015**, *33*, 1048–1057.

(9) (a) Andreu-Vieyra, C. V.; Berenson, J. R. The potential of panobinostat as a treatment option in patients with relapsed and refractory multiple myeloma. *Ther. Adv. Hematol.* **2014**, *5*, 197–210. (b) Ganai, S. A. Novel approaches towards designing of isoform-selective inhibitors against class II histone deacetylases: The acute requirement for targeted anticancer therapy. *Curr. Top. Med. Chem.* **2016**, *16*, 2441–2452.

(10) (a) Stiborova, M.; Eckschlager, T.; Poljakova, J.; Hrabeta, J.; Adam, V.; Kizek, R.; Frei, E. The synergistic effects of DNA-targeted chemotherapeutics and histone deacetylase inhibitors as therapeutic strategies for cancer treatment. *Curr. Med. Chem.* **2012**, *19*, 4218–4238. (b) Ong, P. S.; Wang, X. Q.; Lin, H. S.; Chan, S. Y.; Ho, P. C. Synergistic effects of suberoylanilide hydroxamic acid combined with cisplatin causing cell cycle arrest independent apoptosis in platinum-resistant ovarian cancer cells. *Int. J. Oncol.* **2012**, *40*, 1705–1713.

(11) Santo, L.; Hideshima, T.; Kung, A. L.; Tseng, J. C.; Tamang, D.; Yang, M.; Jarpe, M.; van Duzer, J. H.; Mazitschek, R.; Ogier, W. C.; Cirstea, D.; Rodig, S.; Eda, H.; Scullen, T.; Canavese, M.; Bradner, J.; Anderson, K. C.; Jones, S. S.; Raje, N. Preclinical activity, pharmacodynamic, and pharmacokinetic properties of a selective HDAC6 inhibitor, ACY-1215, in combination with bortezomib in multiple myeloma. *Blood* **2012**, *119*, 2579–2589.

(12) (a) Lee, J. H.; Mahendran, A.; Yao, Y.; Ngo, L.; Venta-Perez, G.; Choy, M. L.; Kim, N.; Ham, W. S.; Breslow, R.; Marks, P. A. Development of a histone deacetylase 6 inhibitor and its biological effects. *Proc. Natl. Acad. Sci. U. S. A.* **2013**, *110*, 15704–15719. (b) Goracci, L.; Deschamps, N.; Randazzo, G. M.; Petit, C.; Dos Santos Passos, C.; Carrupt, P. A.; Simoes-Pires, C.; Nurisso, A. A rational approach for the identification of non-hydroxamate HDAC6-selective inhibitors. *Sci. Rep.* **2016**, *6*, 29086. (c) Wagner, F. F.; Olson, D. E.; Gale, J. P.; Kaya, T.; Weiwer, M.; Aidoud, N.; Thomas, M.; Davoine, E. L.; Lemerrier, B. C.; Zhang, Y. L.; Holson, E. B. Potent and selective inhibition of histone deacetylase 6 (HDAC6) does not require a surface-binding motif. *J. Med. Chem.* **2013**, *56*, 1772–1776. (d) Senger, J.; Melesina, J.; Marek, M.; Romier, C.; Oehme, L.; Witt, O.; Sippl, W.; Jung, M. Synthesis and biological investigation of oxazole hydroxamates as highly selective histone deacetylase 6 (HDAC6) inhibitors. *J. Med. Chem.* **2016**, *59*, 1545–1555. (e) Bergman, J. A.; Woan, K.; Perez-Villaruel, P.; Villagra, A.; Sotomayor, E. M.; Kozikowski, A. P. Selective histone deacetylase 6 inhibitors bearing substituted urea linkers inhibit melanoma cell growth. *J. Med. Chem.* **2012**, *55*, 9891–9899. (f) Butler, K. V.; Kalin, J.; Brochier, C.; Vistoli, G.; Langley, B.; Kozikowski, A. P. Rational design and simple chemistry yield a superior, neuroprotective

HDAC6 inhibitor, tubastatin A. *J. Am. Chem. Soc.* **2010**, *132*, 10842–10856.

(13) Dallavalle, S.; Pisano, C.; Zunino, F. Development and therapeutic impact of HDAC6-selective inhibitors. *Biochem. Pharmacol.* **2012**, *84*, 756–765.

(14) Marek, L.; Hamacher, A.; Hansen, F. K.; Kuna, K.; Gohlke, H.; Kassack, M. U.; Kurz, T. Histone deacetylase (HDAC) inhibitors with a novel connecting unit linker region reveal a selectivity profile for HDAC4 and HDAC5 with improved activity against chemoresistant cancer cells. *J. Med. Chem.* **2013**, *56*, 427–436.

(15) Lobera, M.; Madauss, K. P.; Pohlhaus, D. T.; Wright, Q. G.; Trocha, M.; Schmidt, D. R.; Baloglu, E.; Trump, R. P.; Head, M. S.; Hofmann, G. A.; Murray-Thompson, M.; Schwartz, B.; Chakravorty, S.; Wu, Z.; Mander, P. K.; Kruidenier, L.; Reid, R. A.; Burkhardt, W.; Turunen, B. J.; Rong, J. X.; Wagner, C.; Moyer, M. B.; Wells, C.; Hong, X.; Moore, J. T.; Williams, J. D.; Soler, D.; Ghosh, S.; Nolan, M. A. Selective class IIa histone deacetylase inhibition via a nonchelating zinc-binding group. *Nat. Chem. Biol.* **2013**, *9*, 319–325.

(16) Diedrich, D.; Hamacher, A.; Gertzen, C. G.; Alves Avelar, L. A.; Reiss, G. J.; Kurz, T.; Gohlke, H.; Kassack, M. U.; Hansen, F. K. Rational design and diversity-oriented synthesis of peptoid-based selective HDAC6 inhibitors. *Chem. Commun.* **2016**, *52*, 3219–3222.

(17) Hai, Y.; Christianson, D. W. Histone deacetylase 6 structure and molecular basis of catalysis and inhibition. *Nat. Chem. Biol.* **2016**, *12*, 741–747.

(18) Miyake, Y.; Keusch, J. J.; Wang, L.; Saito, M.; Hess, D.; Wang, X.; Melancon, B. J.; Helquist, P.; Gut, H.; Matthias, P. Structural insights into HDAC6 tubulin deacetylation and its selective inhibition. *Nat. Chem. Biol.* **2016**, *12*, 748–754.

(19) Gohlke, H.; Klebe, G. DrugScore meets CoMFA: adaptation of fields for molecular comparison (AFMoC) or how to tailor knowledge-based pair-potentials to a particular protein. *J. Med. Chem.* **2002**, *45*, 4153–4170.

(20) Sottriffer, C. A.; Gohlke, H.; Klebe, G. Docking into knowledge-based potential fields: a comparative evaluation of DrugScore. *J. Med. Chem.* **2002**, *45*, 1967–1970.

(21) (a) Romine, J. L.; Martin, S. W.; Meanwell, N. A.; Epperson, J. R. Synthesis of 3-Hydroxyisopyrimidine-2,4-diones. Addition of anilines to benzyloxy isocyanate synthons to give N-hydroxyureas. *Synthesis* **1994**, *1994*, 846–850. (b) Khankischpur, M.; Hansen, F. K.; Geffken, D. Convenient synthesis of 5-substituted 2-Amino[1,2,4]triazolo[1,5-a][1,3,5]triazin-7(6H)-ones from N-triazolide imidates and 1,2,4-triazole-3,5-diamine. *Synthesis* **2010**, No. 10, 1645–1648.

(22) (a) Gaisina, I. N.; Tueckmantel, W.; Ugolkov, A.; Shen, S.; Hoffen, J.; Dubrovskiy, O.; Mazar, A.; Schoon, R. A.; Billadeau, D.; Kozikowski, A. P. Identification of HDAC6-selective inhibitors of low cancer cell cytotoxicity. *ChemMedChem* **2016**, *11*, 81–92. (b) Lienlaf, M.; Perez-Villaruel, P.; Knox, T.; Pabon, M.; Sahakian, E.; Powers, J.; Woan, K. V.; Lee, C.; Cheng, F.; Deng, S.; Smalley, K. S.; Montecino, M.; Kozikowski, A.; Pinilla-Ibarz, J.; Sarnaik, A.; Seto, E.; Weber, J.; Sotomayor, E. M.; Villagra, A. Essential role of HDAC6 in the regulation of PD-L1 in melanoma. *Mol. Oncol.* **2016**, *10*, 735–750.

(23) Asgar, M. A.; Senawong, G.; Sripa, B.; Senawong, T. Synergistic anticancer effects of cisplatin and histone deacetylase inhibitors (SAHA and TSA) on cholangiocarcinoma cell lines. *Int. J. Oncol.* **2016**, *48*, 409–420.

(24) Duque-Afonso, J.; Yalcin, A.; Berg, T.; Abdelkarim, M.; Heidenreich, O.; Lubbert, M. The HDAC class I-specific inhibitor entinostat (MS-275) effectively relieves epigenetic silencing of the LAT2 gene mediated by AML1/ETO. *Oncogene* **2011**, *30*, 3062–3072.

(25) Zingle, C.; Kuntz, L.; Tritsch, D.; Grosdemange-Billiard, C.; Rohmer, R. Isoprenoid biosynthesis via the methylerythritol phosphate pathway: structural variations around phosphonate anchor and spacer of fosmidomycin, a potent inhibitor of deoxyxylulose phosphate reductoisomerase. *J. Org. Chem.* **2010**, *75*, 3203–3207.

(26) Ugwuegbulam, C. O.; Foy, J. E. Process for the preparation of anti-malarial drugs. US6479660 (B1), 2002.

(27) Mills, N. ChemDraw Ultra 10.0. *J. Am. Chem. Soc.* **2006**, *128*, 13649–13650 (Computer software review).

(28) Gerber, P. R.; Muller, K. MAB, a generally applicable molecular force field for structure modelling in medicinal chemistry. *J. Comput.-Aided Mol. Des.* **1995**, *9*, 251–268.

(29) Millard, C. J.; Watson, P. J.; Celardo, I.; Gordiyenko, Y.; Cowley, S. M.; Robinson, C. V.; Fairall, L.; Schwabe, J. W. Class I HDACs share a common mechanism of regulation by inositol phosphates. *Mol. Cell* **2013**, *51*, 57–67.

(30) Burlli, R. W.; Luckhurst, C. A.; Aziz, O.; Matthews, K. L.; Yates, D.; Lyons, K. A.; Beconi, M.; McAllister, G.; Breccia, P.; Stott, A. J.; Penrose, S. D.; Wall, M.; Lamers, M.; Leonard, P.; Muller, I.; Richardson, C. M.; Jarvis, R.; Stones, L.; Hughes, S.; Wishart, G.; Haughan, A. F.; O'Connell, C.; Mead, T.; McNeil, H.; Vann, J.; Mangette, J.; Maillard, M.; Beaumont, V.; Munoz-Sanjuan, I.; Dominguez, C. Design, synthesis, and biological evaluation of potent and selective class IIa histone deacetylase (HDAC) inhibitors as a potential therapy for Huntington's disease. *J. Med. Chem.* **2013**, *56*, 9934–9954.

(31) Decroos, C.; Clausen, D. J.; Haines, B. E.; Wiest, O.; Williams, R. M.; Christianson, D. W. Variable active site loop conformations accommodate the binding of macrocyclic largazole analogues to HDAC8. *Biochemistry* **2015**, *54*, 2126–2135.

(32) (a) Osterberg, F.; Morris, G. M.; Sanner, M. F.; Olson, A. J.; Goodsell, D. S. Automated docking to multiple target structures: incorporation of protein mobility and structural water heterogeneity in AutoDock. *Proteins: Struct., Funct., Genet.* **2002**, *46*, 34–40. (b) Morris, G. M.; Goodsell, D. S.; Halliday, R. S.; Huey, R.; Hart, W. E.; Belew, R. K.; Olson, A. J. Automated docking using a Lamarckian genetic algorithm and an empirical binding free energy function. *J. Comput. Chem.* **1998**, *19*, 1639–1662.

(33) (a) Radestock, S.; Bohm, M.; Gohlke, H. Improving binding mode predictions by docking into protein-specific adapted potential fields. *J. Med. Chem.* **2005**, *48*, 5466–5479. (b) Gohlke, H.; Hendlich, M.; Klebe, G. Knowledge-based scoring function to predict protein-ligand interactions. *J. Mol. Biol.* **2000**, *295*, 337–356.

(34) Gediya, L. K.; Chopra, P.; Purushottamachar, P.; Maheshwari, N.; Njar, V. C. A new simple and high-yield synthesis of suberoylanilide hydroxamic acid and its inhibitory effect alone or in combination with retinoids on proliferation of human prostate cancer cells. *J. Med. Chem.* **2005**, *48*, 5047–5051.

(35) Gosepath, E. M.; Eckstein, N.; Hamacher, A.; Servan, K.; von Jonquieres, G.; Lage, H.; Gyorffy, B.; Royer, H. D.; Kassack, M. U. Acquired cisplatin resistance in the head-neck cancer cell line Cal27 is associated with decreased DKK1 expression and can partially be reversed by overexpression of DKK1. *Int. J. Cancer* **2008**, *123*, 2013–2019.

(36) Eckstein, N.; Servan, K.; Girard, L.; Cai, D.; von Jonquieres, G.; Jaehde, U.; Kassack, M. U.; Gazdar, A. F.; Minna, J. D.; Royer, H. D. Epidermal growth factor receptor pathway analysis identifies amphiregulin as a key factor for cisplatin resistance of human breast cancer cells. *J. Biol. Chem.* **2008**, *283*, 739–750.

(37) (a) Heltweg, B.; Trapp, J.; Jung, M. In vitro assays for the determination of histone deacetylase activity. *Methods* **2005**, *36*, 332–337. (b) Wegener, D.; Wirsching, F.; Riestler, D.; Schwienhorst, A. A fluorogenic histone deacetylase assay well suited for high-throughput activity screening. *Chem. Biol.* **2003**, *10*, 61–68.

(38) Heltweg, B.; Dequiedt, F.; Verdin, E.; Jung, M. Nonisotopic substrate for assaying both human zinc and NAD⁺-dependent histone deacetylases. *Anal. Biochem.* **2003**, *319*, 42–48.

(39) Marek, M.; Kannan, S.; Hauser, A. T.; Moraes Mourao, M.; Caby, S.; Cura, V.; Stofa, D. A.; Schmidtkunz, K.; Lancelot, J.; Andrade, L.; Renaud, J. P.; Oliveira, G.; Sippl, W.; Jung, M.; Cavarelli, J.; Pierce, R. J.; Romier, C. Structural basis for the inhibition of histone deacetylase 8 (HDAC8), a key epigenetic player in the blood fluke *Schistosoma mansoni*. *PLoS Pathog.* **2013**, *9*, e1003645.

(40) Engelke, L. H.; Hamacher, A.; Proksch, P.; Kassack, M. U. Ellagic acid and resveratrol prevent the development of cisplatin resistance in the epithelial ovarian cancer cell line A2780. *J. Cancer* **2016**, *7*, 353–363.

(41) Ciossek, T.; Julius, H.; Wieland, H.; Maier, T.; Beckers, T. A homogeneous cellular histone deacetylase assay suitable for compound profiling and robotic screening. *Anal. Biochem.* **2008**, *372*, 72–81.

(42) Bonfils, C.; Kalita, A.; Dubay, M.; Siu, L. L.; Carducci, M. A.; Reid, G.; Martell, R. E.; Besterman, J. M.; Li, Z. Evaluation of the pharmacodynamic effects of MGCD0103 from preclinical models to human using a novel HDAC enzyme assay. *Clin. Cancer Res.* **2008**, *14*, 3441–3449.

(43) Hoffmann, K.; Brosch, G.; Loidl, P.; Jung, M. A non-isotopic assay for histone deacetylase activity. *Nucleic Acids Res.* **1999**, *27*, 2057–2058.

(44) Schneider, C. A.; Rasband, W. S.; Eliceiri, K. W. NIH Image to ImageJ: 25 years of image analysis. *Nat. Methods* **2012**, *9*, 671–675.